Available online at www.sciencedirect.com
ScienceDirect
Geochimica et Cosmochimica Acta 71 (2007) 2299–2325
Geochimica et Cosmochimica Acta
www.elsevier.com/locate/gca

Origin of retrograde fluid in ultrahigh-pressure metamorphic rocks: Constraints from mineral hydrogen isotope and water content changes in eclogite–gneiss transitions in the Sulu orogen

Ren-Xu Chen, Yong-Fei Zheng *, Bing Gong, Zi-Fu Zhao, Tian-Shan Gao, Bin Chen, Yuan-Bao Wu

CAS Key Laboratory of Crust-Mantle Materials and Environments, School of Earth and Space Sciences, University of Science and Technology of China, Hefei 230026, China

Received 1 June 2006; accepted in revised form 15 February 2007; available online 23 February 2007

Abstract

By taking advantage of having depth profiles between contrasting lithologies from core samples of the Chinese Continental Scientific Drilling (CCSD) project, a combined study was carried out to examine changes in mineral H isotope, total water and hydroxyl contents in garnet and omphacite across the contacts between ultrahigh-pressure (UHP) eclogite and gneiss in the Sulu orogen, east-central China. The samples of interest were from two continuous core segments from the CCSD main hole at depths of 734.21–737.16 and 929.67–932.86 m, respectively. The results show δD values of −116‰ to − 64‰ for garnet and −104‰ to −82‰ for omphacite, consistent with incorporation of meteoric water into protoliths of UHP metamorphic rocks by high-T alteration. Both equilibrium and disequilibrium H isotope fractionations were observed between garnet and omphacite, suggesting fluid-assisted H isotope exchange at local scales during amphibolite-facies retrogression. While bulk water analysis gave total H_2O concentrations of 522–1584 ppm for garnet and 1170–20745 ppm for omphacite, structural hydroxyl analysis yielded H_2O contents of 80–413 ppm for garnet and 228–412 ppm for omphacite. It appears that significant amounts of molecular H_2O are present in the minerals, pointing to enhanced capacity of water storage in the UHP eclogite minerals. Hydrogen isotope variations in the transition between eclogite and gneiss show correlations with variations in their water contents. Petrographically, the degree of retrograde metamorphism generally increases with decreasing distance from the eclogite–gneiss boundary. Thus, retrograde metamorphism results in mineral reactions and H isotope variation. Because hydroxyl solubility in nominally anhydrous minerals decreases with dropping pressure, significant amounts of water are expected to be released from the minerals during decompression exhumation. Decompression exsolution of structural hydroxyl from 1 m^3 volume of eclogite composed of only garnet and omphacite results in release of a quantitative estimate of 3.07–3.44 kg water that can form 140–156 kg amphibole during exhumation. Therefore, it is concluded that fluid for retrogression of the eclogites away from the eclogite–gneiss boundary was derived from the decompression exsolution of structural hydroxyl and molecular H_2O in nominally anhydrous minerals. For the eclogites adjacent to gneiss, in contrast, the retrograde metamorphism was principally caused by aqueous fluid from the gneiss which is relatively rich in water. Consequently, both the origin and availability of metamorphic fluid during exhumation of deeply subducted continental crust are deciphered by this combined study focusing on the transitions and the retrograde processes between the felsic and mafic UHP rocks.

* Corresponding author. Fax: +86 551 3603554.
E-mail address: yfzheng@ustc.edu.cn (Y.-F. Zheng).

0016-7037/$ - see front matter © 2007 Elsevier Ltd. All rights reserved.
doi:10.1016/j.gca.2007.02.012

1. INTRODUCTION

Since findings of coesite and diamond in metamorphic rocks from the Dabie-Sulu orogenic belt in east-central China (e.g., Okay et al., 1989; Wang et al., 1989; Xu et al., 1992), this region has been one of the most important targets for studying ultrahigh-pressure (UHP) metamorphism during continental collision (cf. Zheng et al., 2003; and references therein). In the past decade, significant progress concerning the role of fluids during UHP metamorphism has been made. Hydrous minerals, such as phengite, zoisite, talc, amphibole, and topaz were found to be stable under UHP metamorphic conditions (e.g., Liou et al., 1995; Zhang et al., 1995, 2000, 2002). Since findings of unusually negative $\delta^{18}O$ values for minerals from UHP eclogite at Qinglongshan (Yui et al., 1995; Zheng et al., 1996), a great deal of stable isotope studies have been devoted to investigation of both the distribution and origin of widespread ^{18}O depletion in both mafic and felsic UHP metamorphic rocks from this orogenic belt (Baker et al., 1997; Yui et al., 1997; Rumble and Yui, 1998; Zheng et al., 1998, 1999, 2004; Fu et al., 1999; Rumble et al., 2002). Studies of petrology and fluid inclusions were also carried out, mostly in combination with stable isotope analyses, to decipher fluid regimes in the UHP metamorphic rocks (Xiao et al., 2000, 2001, 2002; Franz et al., 2001; Fu et al., 2001, 2002, 2003a,b; Li et al., 2004). Xiao et al. (2000) reported early Ca-rich brines which may have originated during prograde metamorphism; NaCl-rich fluids may have been trapped during the peak of UHP metamorphism. Fu et al. (2003a) distinguished different generations of fluid inclusions in the UHP rocks: pre- to syn-peak metamorphic fluids, consisting of N_2, CH_4 and high salinity brines, and post-peak metamorphic fluids rich in CO_2 and low-salinity water. More interesting is the observation that considerable amounts of water were measured in nominally anhydrous minerals such as garnet and omphacite in the Dabie-Sulu UHP rocks (Zhang et al., 2001, 2004; Su et al., 2002, 2004; Xia et al., 2005; Sheng et al., 2007). The occurrence of the fluids indicates that the UHP metamorphism proceeded with variable degrees of fluid–rock interaction but with limited mobility of aqueous fluids during subduction and exhumation.

Although, it is well known that fluids play important roles during subduction of young and hot oceanic crust (e.g., Touret, 2001; Miller et al., 2002; Schmidt and Poli, 2003), less is known about fluid availability during subduction and exhumation of old and cold continental crust (Zheng et al., 2003). Petrological and geochemical studies of surface samples have provided important constraints on fluid availability during pre- to syn-UHP metamorphism. However, there is little known about fluid behavior during exhumation, especially about the origin of retrograde fluid. The Chinese Continental Scientific Drilling (CCSD) in Donghai of the Dabie-Sulu UHP metamorphic belt is aiming to reconstruct the formation and exhumation mechanisms of UHP metamorphic terranes; one of the major goals is to investigate variation in fluid composition with depth, flow patterns and cycling mechanisms, as well as changes in fluid regime with time (Xu et al., 1998). Oxygen isotope and fluid inclusion distributions through vertical sections from 100 to 3000 m of the CCSD main hole have been investigated by Xiao et al. (2006) and Zhao et al. (2007). This paper presents a combined study of petrological observations, hydrogen isotopes and water concentrations (total H_2O and structural hydroxyl) in garnet and omphacite from two continuous core segments consisting of eclogite and gneiss from the CCSD main hole. The results provide geochemical constraints on fluid behavior during the exhumation of deeply subducted continental crust.

2. GEOLOGICAL SETTING AND SAMPLES

The Dabie-Sulu orogenic belt in east-central China was formed by the continental collision between the South China Block and the North China Block in the Triassic (e.g., Wang et al., 1995; Cong, 1996; Liou et al., 1996; Li et al., 1999; Zheng et al., 2005a). It is separated into two terranes by approximately 500 km of left-lateral strike-slip displacement along the Tan-Lu fault (Fig. 1). The Sulu orogen in the east is separated from the North China Block to the NW by the Wulian–Qingdao–Yantai Fault (WQYF), and the South China Block to the SE by the Jiashan–Xiangshui Fault (JXF). The Sulu UHP and HP belt extends for about 320 km from Weihai in northeastern Shandong province to Donghai in northern Jiangsu province (Fig. 1). The metamorphic rocks in this UHP belt are predominantly amphibolite-facies orthogneisses, paragneisses, amphibolite and marble; some gneissic rocks and marble contain abundant eclogite layers and blocks. Evidence for UHP metamorphism has been recognized in coesite-bearing eclogite, schist, ultramafic rocks, and some country rock gneisses (Enami et al., 1995; Zhang et al., 1995; Liou and Zhang, 1996; Ye et al., 2000; Liu et al., 2004a,b). The HP belt, southeast of the UHP belt, consists mainly of quartz–mica schist, chloritoid–kyanite–mica–quartz schist, marble, and rare blueschist (Zhang et al., 1995).

CCSD-MH, the main hole of the Chinese Continental Scientific Drilling Project, with a depth 5158.8 m, is located at 34°25′N, 118°40′E near the village of Maobei, about 17 km SW of Donghai county in Jiangsu province (Fig. 1). This area is underlain mainly by orthogneiss and supercrustal rocks mostly with Neoproterozoic protolith ages (Liu et al., 2004a,b; Zheng et al., 2004). They were intruded by Cretaceous granite and unconformably overlain by Quaternary sedimentary cover (Fig. 1). Findings of coesite in gneiss and eclogite in this area (Liu et al., 2004a,b) and diamond in eclogite from Maobei (Xu et al., 2003, 2005) demonstrate that the high-grade rocks in this area were subducted to mantle depths to undergo UHP metamorphism. CCSD-MH is located at the Maobei eclogite complex, SW of the Maobei shear tectonic sliver. The rocks on the surface are predominantly gneiss, eclogite, schist, amphibolite, peridotite, mylonite and cataclasite. The widespread eclogites occur as pods or layers ranging from <1 m to hundreds of meters in length, and the direct country rocks are mafic-ultramafic rocks, marble and gneiss.

No core sample was recovered in the uppermost 100 m of the CCSD main hole; only slushy fragments were

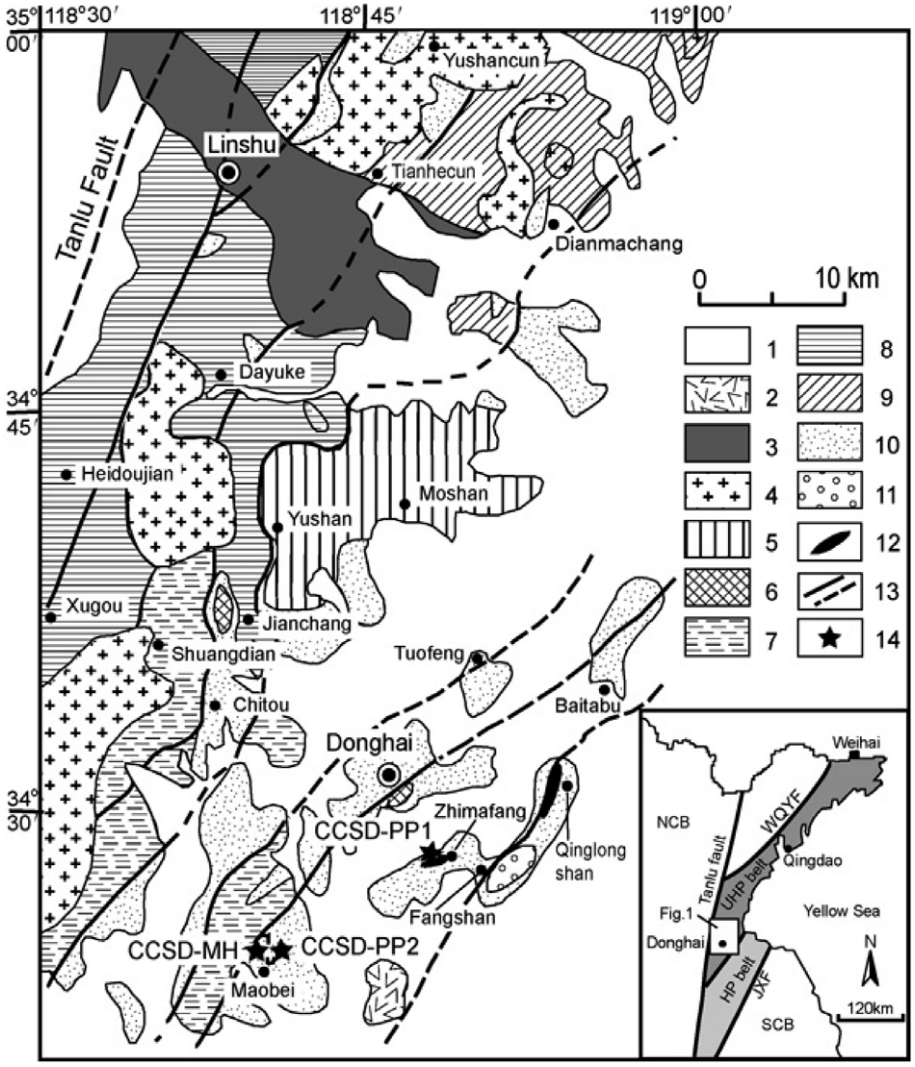

Fig. 1. Sketch map of the geology in the Sulu orogen and the Donghai area, showing major lithotectonic units and the locations of outcrops and pre-pilot drillhole of CCSD-PP1, CCSD-PP2 and the CCSD main hole (modified after Liu et al., 2001). (1) Quaternary; (2) tertiary basalt; (3) Cretaceous basin; (4) Cretaceous granite; (5) aegirine-bearing granitic gneiss; (6) amphibole-bearing granitic gneiss; (7) garnet-bearing granitic gneiss; (8) biotite-bearing granitic gneiss; (9) amphibole-bearing and biotite-bearing granitic gneiss; (10) epidote-bearing and biotite bearing granitic gneiss; (11) supracrustal rocks, including paragneisses, kyanite-bearing and jadeite-bearing quartzite, and marble; (12) eclogite and ultramafic rocks; (13) ductile shear zone or fault; (14) drilling hole. NCB, North China Block; SCB, South China Block; WQYF, Wulian–Qingdao–Yantai fault; JXF, Jiashan–Xiangshui fault.

obtained. The 100–2050 m of the main hole mainly consists of eclogite-facies rocks with a cumulative thickness of about 1200 m. The rocks are predominantly orthogneiss, paragneiss, eclogite, garnet peridotite and rare schist and quartzite (Zhang et al., 2006). According to their special distribution, occurrence, rock association and compositional variation, the rocks from 100 to 2050 m can be divided into six lithological units (Fig. 2; Zhang et al., 2006). With increasing depths, they are as follows: unit 1 (from 100 to 530 m) consists mainly of quartz-rich eclogite, intercalated layers of rutile-rich eclogite and thin layers of paragneiss; unit 2 (from 530 to 600 m) is composed mainly of rutile- and ilmenite-rich eclogite; unit 3 (from 600 to 680 m) consists of ultramafic rock with minor eclogites and garnet clinopyroxenite as thin layers and blocks; unit 4 (from 695 to 1160 m) is composed mainly of interlayered paragneiss, eclogite and retrograded eclogite (amphibolite), and a thin layer of ultramafic rock; unit 5 (from 1160 to 1600 m) consists mainly of orthogneiss with thin layers of paragneiss and eclogite; and unit 6 (from 1600 to 2050 m) consists mainly of eclogite with minor paragneisses occurring as an interlayer in the middle part of the unit.

The two continuous core segments, 02CCSD-I and 02CCSD-II, used in this study were obtained from the CCSD main hole. Both of them are 3 m long and were obtained at depths of 734.21–737.16 and 929.67–932.86 m, respectively. They belong to the fourth rock unit in which the eclogites occur as an interlayer in the gneiss. Most of the eclogites from the two core segments have low SiO_2 of 47–55%, $Na_2O + K_2O$ of 2.3–4.3%, Al_2O_3 of 15–20%,

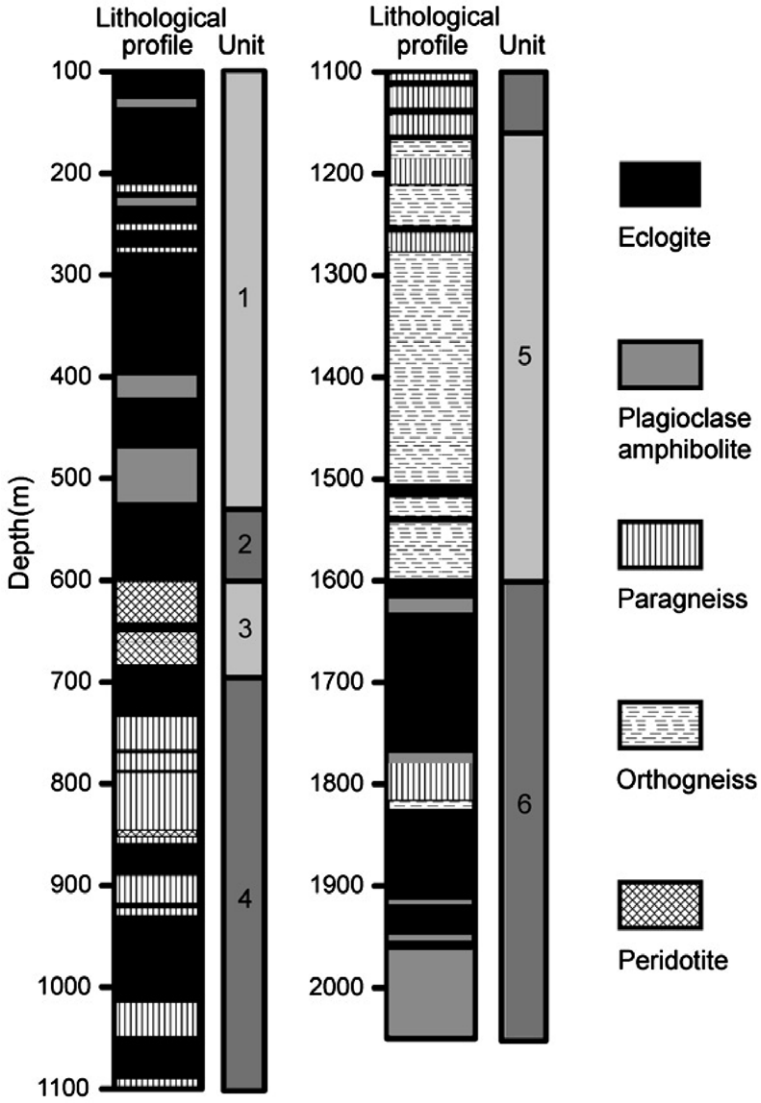

Fig. 2. Lithological profile of CCSD main hole from depths of 100 to 2050 m (revised after Zhang et al., 2006).

and FeO^T of 8–16% (Zhang et al., 2006). These two core segments are separated by a ductile shear zone (Fig. 3), and the second core segment, 02CCSD-II, is located in the shear zone with a thickness of ~300 m (Xu et al., 2004). The gneisses of the two core segments both have undergone UHP metamorphism, as shown by the occurrence of coesite inclusion in zircon from the gneiss and, in some cases, garnet and phengite inclusions (Liu et al., 2004a,b). This indicates that the relationship between eclogite and associated gneiss is "in situ". SHRIMP U–Pb dating for coesite-bearing domains of zircons from the CCSD gneisses yields ages of 226–234 Ma for the UHP metamorphic event and about 750–780 Ma for the host metaigneous protolith (Liu and Xu, 2004; Liu et al., 2004a,b). These dates are consistent with known results from multi-method geochronological studies of surface-exposed UHP metamorphic rocks along the Dabie-Sulu orogenic belt (e.g., Ames et al., 1996; Hacker et al., 1998, 2000; Li et al., 1999, 2000, 2004; Zheng et al., 2003, 2004, 2005b). In particular, SHRIMP zircon U–Pb dating yields a range of 242 ± 2 to 227 ± 2 Ma for UHP metamorphism in the field of coesite stability (Wu et al., 2006). A combined study of petrography and geochronology for the CCSD-MH eclogite also reveals the occurrence of an HP eclogite-facies recrystallization phase at 216 ± 3 Ma (Zhao et al., 2006).

3. ANALYTICAL METHODS

3.1. TC/EA-MS analysis

Minerals were separated for isotopic analyses. After crushing, a shaking bed was used to separate heavy minerals, followed by magnetic separation using a magnetic separator, and then purification by hand picking under binocular microscopes. All mineral separates used for H isotope analyses were grained in sizes of 40–60 μm.

Hydrogen isotope composition and H_2O concentration in minerals were simultaneously analyzed by the

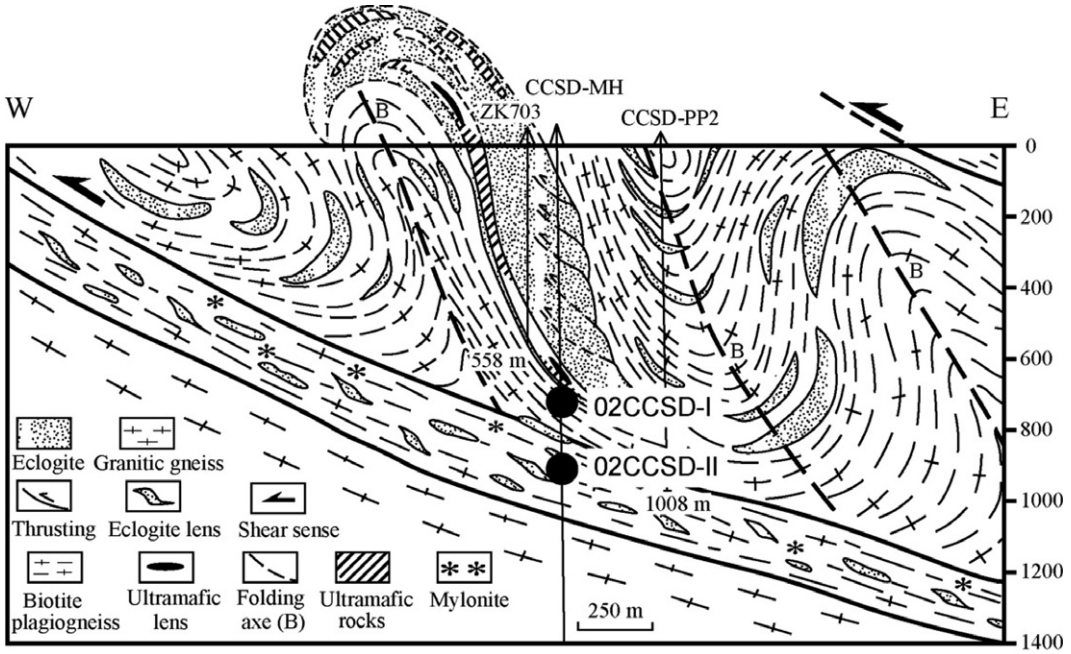

Fig. 3. Sketch model of tectonics for the Chinese Continental Scientific Drilling (CCSD) sites above 1200 m (after Xu et al., 2004). CCSD-MH and CCSD-PP2 denote the main hole and pilot hole of CCSD, and ZK-703 denotes a shallow hole.

TC/EA-MS online technique at the University of Science and Technology of China in Hefei (Gong et al., 2007a). This is an integrated procedure that uses a thermal conversion elemental analyzer (TC/EA) and isotope-ratio mass spectrometer (MS) with a continuous flow inlet system. Similar analytical procedures have been described for organic and inorganic compounds (e.g., Begley and Scrimgeour, 1997; Hilkert et al., 1999; Eiler and Kitchen, 2001; Sharp et al., 2001; Godin et al., 2004). Because water is present in the forms of both molecular H_2O and structural hydroxyl in hydrous and nominally anhydrous minerals, total H_2O concentration was measured by the TC/EA-MS method. In our online analysis, nevertheless, reduction furnace and gas chromatography in a Finnigan TC/EA were combined with a MAT-253 mass spectrometer via an open split in Finnigan Conflo III interface. The reduction column consists of an 18 mm diameter ceramic tube lined with a glassy carbon sleeve. A temperature of 1450 °C was used for the carbon reduction in order to warrant better precision for inorganic solid samples (Sharp et al., 2001) and a longer life of the reduction furnace (Burgoyne and Hayes, 1998). Solid samples were wrapped in silver foil capsules and dropped into the furnace using an autosampler. All inorganic solid samples were preheated at 90 °C for 12 h to eliminate adsorption water on sample surfaces. Both H_2 and CO gases were produced by the reaction of H_2O and C in a He carrier gas. They were separated in the gas chromatograph (GC) and then analyzed in the mass spectrometer using the continuous flow mode. When H_2 was analyzed, GC was operated at 90 °C to reduce the retention time and minimize peak broadening. When not in use, it was heated to 300 °C with a low-flow He stream for cleaning.

In addition to determining D/H ratios, the time-integrated intensity of sample peak was used to determine wt% or ppm wt H_2O. This was done by measuring a reference material to obtain a k-factor according to the following relation:

$$k = \frac{w_{\mathrm{ref}} * m_{\mathrm{ref}}}{A_{\mathrm{ref}}} \quad (1)$$

where w_{ref} and m_{ref} are the reference weight percent and mass, respectively; A_{ref} is the reference peak area emerged from the measurement. A_{ref} can be used by blank-correction to enhance the precision of k-factor calculation. Then the k-factor just calculated was used to obtain the sample's weight percent w_{sample} following the equation:

$$w_{\mathrm{sample}} = \frac{k * A_{\mathrm{sample}}}{m_{\mathrm{sample}}} \quad (2)$$

where w_{sample} and m_{sample} are the sample's weight percent and mass, respectively; A_{sample} is the sample's peak area emerged from the measurement. In our analysis, after a reference material was measured as the reference, the other two reference materials were also measured to check the validity of the k-factor.

The ^{4}He tailing was eliminated by using an electrostatic filter in MAT-253. The mass 3 [m_3] signal has contributions from both HD and H_3^+ ions. The formation of H_3^+ ions comes from ion molecule reactions between H_2^+ and neutral H_2 in the ion source. As the contribution of H_3^+ ions relates to the amount of H_2 in the ion source, a correction factor (H_3^+-factor) can be determined by measuring the apparent D/H ratios for H_2 gas pulses of different intensity. The H^{3+}-factor was calculated by the Finnigan MAT ISODAT software for the H^{3+} ion correction. In our analysis,

there was not a measurable blank associated with sample introduction, but there was a measurable blank from the silver foil capsules themselves. This can be eliminated by blank-correction.

The measured H isotope ratios are presented in the conventional δD notation relative to VSMOW, and the water contents are presented in H_2O ppm by weight. Two standards were used during the H isotope analyses: $\delta D = -65.7‰$ for NBS-30 biotite, and $\delta D = -100.3‰$ for IAEA-CH-7 Polyethylene. One standard was used for calibration of the H_2O content analyses: 5.0% H (wt) for benzoic acid ($C_7H_6O_2$). A home-standard garnet 04BXL02 was used to control both H isotope and water content analyses; it has a δD value of $-94 \pm 1‰$ and a total H_2O content of 522 ± 11 ppm by weight (Gong et al., 2007a). Our protocols show the routine analysis of sample sizes as small as 0.01 μl H_2O for both H isotope composition and H_2O concentration in hydrous and nominally anhydrous minerals. Depending on mineral water contents, absolute reproducibility for mineral δD value is generally about $\pm 1‰$ to $\pm 2‰$ (1σ) and relative uncertainty for total H_2O concentration is at levels of $\pm 1\%$ to $\pm 3\%$ (1σ). In practice, the respective analytical errors for the δD value and the H_2O content can be as small as $\pm 0.5‰$ and $\pm 0.3\%$ for hydrous minerals, but as large as $\pm 3‰$ and $\pm 5\%$ for nominally anhydrous minerals with low water content.

3.2. FTIR analysis

Concentrations of structural hydroxyl in nominally anhydrous minerals were determined by Fourier Transform Infrared Spectra (FTIR) at the University of Science and Technology of China in Hefei, with analytical procedures similar to those used in previous studies (e.g., Su et al., 2002; Katayama and Nakashima, 2003; Xia et al., 2005). The samples used for the FTIR analysis were prepared as doubly polished sections about 2×1 cm and 0.2–0.4 mm thick. The cleaning procedure included 24 h dissolution of sections in ethanol or acetone, followed by repeated cleaning with ethanol and distilled water. To remove the surface absorbed water, sections were heated in an oven at ~ 100 °C for more than 6 h. Infrared spectra were obtained by a Nicolet5700 FTIR spectrometer equipped with a Continuμm microscope. Measurements were carried out by unpolarized radiation with an IR light source, a KBr beam-splitter and a MCT-A liquid N_2 cooled detector, at room temperature. One-hundred and twenty eight/two-hundred and fifty eight scans at a resolution of 2/4 cm^{-1} were averaged for each analysis. The background was recorded before analyzing each section. IR spectra were measured by a 50×50 μm aperture on "clean" areas without visible inclusions or cracks, but as shown by FTIR, submicroscopic fluid inclusions (<1–2 μm) should exist.

The hydroxyl content of garnet and omphacite was calculated in terms of the Beer-Lambert law as follows:

$$C_{OH} = \frac{1}{I\gamma d}\int_{\nu 2}^{\nu 1} K(\upsilon) \quad (3)$$

where C_{OH} is the water concentration in analyzed minerals and is generally expressed as moles per liter, $K(\upsilon)$ is the absorption intensity (absorbance) of the water as a function of wavenumber υ, I is the integrated molar absorption coefficient, γ is the orientation factor, which depends on crystallographic anisotropy (Paterson, 1982), and d is the sample thickness. The integrated molar absorption coefficient I was determined for specific minerals using one of the other independent calibration methods and an infrared spectrum. The integrated molar absorption coefficient used in this study for garnet is from Bell et al. (1995): 1.39 ppm^{-1} H_2O cm^{-2} and omphacite is from Katayama et al. (2006): $8.34 \pm 1.46 \times 10^4$ (L mol^{-1} cm^{-2}). We take the absorption coefficient for omphacite as determined by Katayama et al. (2006), because it is a mineral specific calibration and our infrared spectra are similar to those from them. Because the precision of thickness of the same section is <10%, for more than 35 measured points covering the whole section for all samples, the average value was used for different grains from the same sample. The orientation factor of 1/3 was applied to omphacite.

The structural hydroxyl contents are also presented in H_2O ppm by weight. The uncertainty in the FTIR determined hydroxyl content comes from: (1) the baseline correction; (2) integrated area calculation (deduction of the contribution of group III bands and sometimes 3730 cm^{-1} bands for garnet); (3) minor difference in thickness for different grains in the same section; (4) absorption coefficient due to the difference in composition between the garnets in this study and those used by Bell et al. (1995), but this effect is very small because the difference among pure end-member garnets is less than ±10% (Rossman and Aines, 1991; Bell et al., 1995). The difference in composition between the omphacites in this study and those used by Katayama et al. (2006) will not import uncertainty either. On these bases, the overall uncertainty is estimated to be about ±10% for garnet and about ±30% for omphacite.

4. RESULTS

4.1. Petrography

4.1.1. First core segment (02CCSD-I)

The first core segment 02CCSD-I comprises a transition between eclogite and gneiss from depths of 734.21–737.16 m (Fig. 2). The eclogite is composed of omphacite, garnet, quartz, phengite, retrogressive amphibole and plagioclase. Accessory minerals are rutile, titanite, ilmenite and zircon. In general, the eclogite has a porphyroblast texture with garnet as the porphyroblast. The eclogite minerals show a remarkable variability of pervasively retrograded texture. Omphacite is usually replaced by very fine-grained symplectites that consist of retrogressive amphibole and plagioclase (Fig. 4b and d). Garnet contains fertile inclusions including omphacite, rutile, diopside, quartz and amphibole; the rims of most garnets are retrograded to edenite/pargasite (Fig. 4b and d). Rutile is commonly rimmed by ilmenite. The eclogites from different fragments of the core segment show different degrees of retrograde metamorphism. Eclogite I-5A and I-7A have the largest extent of retrograde metamorphism as there was no omphacite for FTIR analysis. For eclogite I-6A and two samples of

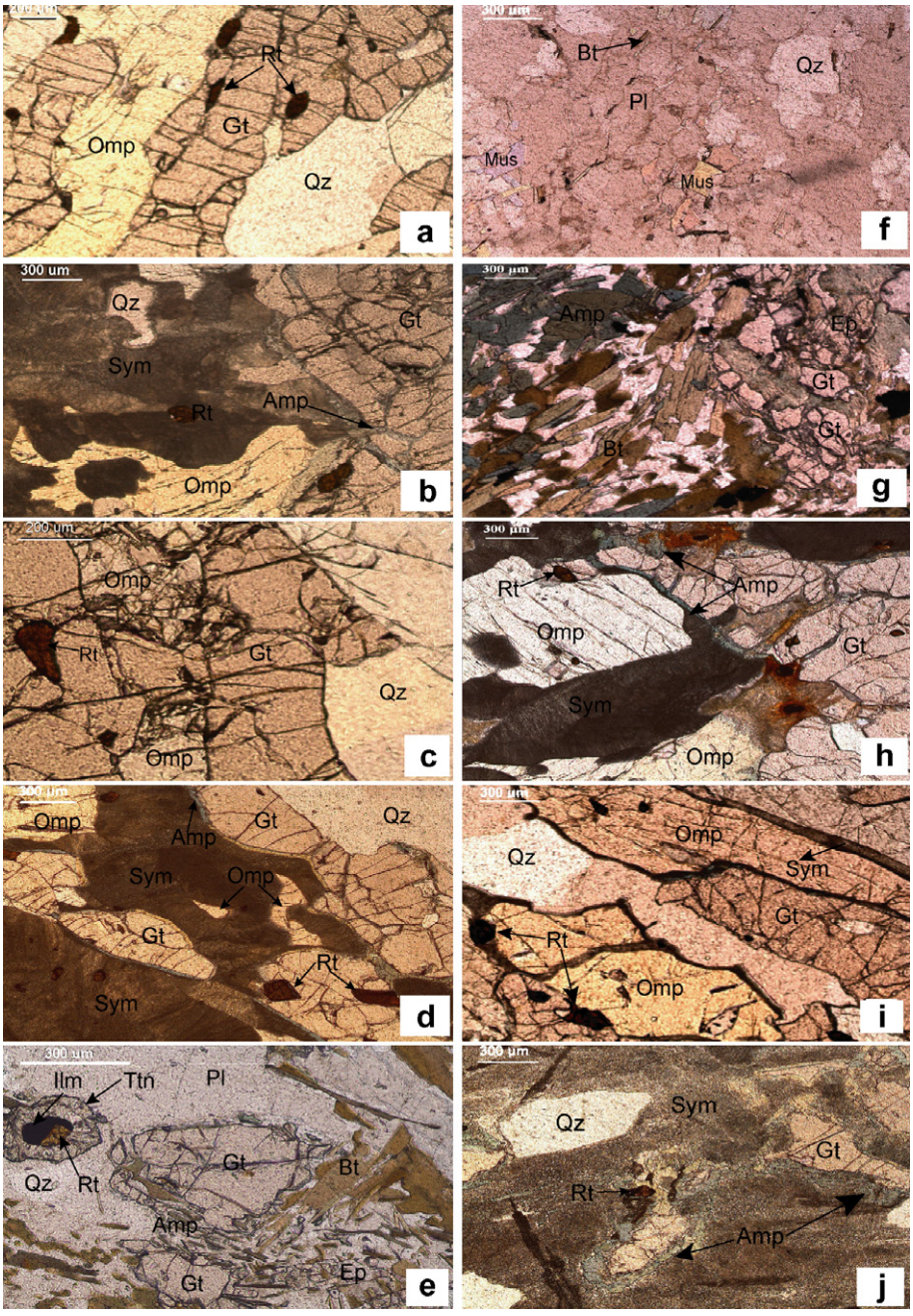

Fig. 4. Microphotographs of eclogite, gneiss and garnet amphibolite from the CCSD main hole. (a) Eclogite (I-12A, 734.78 m), containing garnet, omphacite, phengite, quartz and rutile. (b) Eclogite (I-10A, 735.20 m), containing garnet, omphacite, quartz and rutile. Abundant symplectite was formed after omphacite, garnet is commonly rimmed by symplectite. (c) Eclogite (I-8A, 735.52 m), consisting mainly of garnet, omphacite, quartz, with minor rutile. (d) Eclogite (I-6A, 736.01 m), containing mainly garnet, omphacite, and quartz, with minor rutile, ilmenite and titanite. Most of the omphacite was replaced by symplectite, and garnet was commonly rimmed by symplectite. (e) Gneiss (I-3A, 736.74 m), consisting of quartz, plagioclase, garnet, biotite, amphibole and epidote, with minor rutile, ilmenite and titanite. (f) Gneiss (II-9A, 930.32 m), containing quartz, plagioclase, feldspar, muscovite and biotite. (g) Garnet amphibolite (II-7A, 930.74 m), consisting of garnet, amphibole, biotite, plagioclase and epidote. (h) Eclogite (II-5A, 931.33 m), containing garnet, omphacite, quartz, with minor rutile. Some of the omphacite was replaced by symplectite, and garnet is commonly rimmed by symplectite. (i) Eclogite (II-3A, 932.03 m), consisting of quartz, garnet, omphacite, with minor rutile. (j) Eclogite [II-1(2)A, 932.49 m], containing garnet, omphacite, quartz, with minor rutile. Most of the omphacite was replaced by symplectite, and garnet is commonly rimmed by symplectite. Mineral abbreviations: Gt, garnet; Omp, omphacite; Sym, symplectite; Qz, quartz; Rt, rutile; Ilm, ilmenite; Ttn, titanite; Amp, amphibole; Bt, biotite; Pl, plagioclase; Ep, epidote; Mus, muscovite.

eclogite I-10A and I-11A away from the boundary, most of the omphacites were replaced by the symplectites and garnet are rimmed by edenite/pargasite (Fig. 4b and d). While in the other eclogites, most crystals are fresh. Occasional symplectites occur around the outermost area of omphacite, but no symplectite after garnet was found (Fig. 4a and c).

The gneiss mainly consists of quartz, plagioclase, garnet, epidote, biotite and amphibole, with minor amounts of apatite, rutile, ilmenite and titanite. Sometimes it looks like a retrograde eclogite (Fig. 4e), with relict garnet that is rimmed by a symplectite of amphibole and plagioclase, and relict rutile that was replaced by ilmenite and titanite. But, lithochemically it still belongs to the category of felsic gneiss.

4.1.2. Second core segment (02CCSD-II)

The second core segment, 02CCSD-II, is composed of a transition from gneiss, garnet amphibolite to eclogite from depths of 929.67–932.86 m (Fig. 2). The petrographic feature is different for different rocks of the same rock type and different regions of the same thin section. The petrology of the three rock types is described as follows.

(1) The gneiss has an amphibolite-facies mineral assemblage which consists of quartz, biotite, muscovite, plagioclase, K-feldspar, and amphibole, with minor garnet relict (Fig. 4f).
(2) The garnet amphibolite mainly consists of amphibole, quartz, garnet, apatite, plagioclase, epidote and biotite. Abundant symplectite after the primary omphacite and large amounts of residual garnet can be observed in the garnet amphibolite that is close to the eclogite. In contrast, larger sizes of amphibole grains in symplectite after omphacite/garnet, less residual garnet, more biotite and epidote occur in the garnet amphibolite adjacent to gneiss (Fig. 4g).
(3) The eclogite is mainly composed of garnet, omphacite, quartz, and minor rutile, phengite, plagioclase and K-feldspar. The eclogite minerals show a remarkable variability of pervasively retrograded texture. Eclogite II-1A and II-1(2)A have the largest extent of retrograde metamorphism. Most of the omphacites were replaced by very fine-grained symplectites that consist of retrogressive amphibole and plagioclase; and most garnets are rimmed by retrogressive corona of amphibole (Fig. 4j). The extent of retrograde metamorphism for eclogite II-2A and II-5A are less since only some of the omphacites were replaced by symplectite and only some of the garnets are rimmed by retrogressive sodic amphibole (Fig. 4h). For the other eclogites, II-3A, II-4(1)A and II-4(2)A, most crystals are fresh. Occasionally, symplectites occur around the outermost area of omphacite, but no symplectite after the garnet was found (Fig. 4i).

4.2. Total water

4.2.1. Water content

Total water measured by TC/EA-MS encompasses both molecular H_2O (e.g., fluid inclusions and hydrous phase inclusions) and structural hydroxyl in the minerals. Total water concentrations of garnet and omphacite from the two continuous CCSD-MH core segments are presented in Table 1 and illustrated in Figs. 5, 6 and 8. The eclogite from the first core segment shows total H_2O concentrations of 630–1251 ppm in garnet and 1260–6003 ppm in omphacite, whereas those of garnet from gneiss are 702–963 ppm (Table 1). Eclogites I-8A through I-14A away from the boundary between eclogite and gneiss have homogeneous water contents of ~700 ppm in garnet, whereas garnets from the three samples of eclogites I-5 A through I-7A close to the boundary have significantly higher water contents of 828 to 1251 ppm. Except for sample I-3A, the gneiss has a garnet water content of 801–963 ppm. The content is higher than that in eclogites away from the boundary, but lower than that close to the boundary (Figs. 5c and 8a). Similarly, omphacites from the eclogites close to the boundary have significantly higher water contents than those away from the boundary (Figs. 5c and 8b).

For the second core segment, total H_2O concentrations of garnet and omphacite from eclogite are 522–936 and 1170–10323 ppm, respectively. Garnet from garnet amphibolite and gneiss has water contents of 1035 and 1089–1584 ppm, respectively. Omphacite from the garnet amphibolite has a H_2O concentration of 20745 ppm (Table 1). The water content of garnet from the eclogite is heterogeneous and can be divided into three groups: (1) two samples in the middle of the eclogite II-3A and II-4(1)A have a water content of ~900 ppm; (2) four samples II-1A, II-2A, II-4(2)A and II-5A have a water concentration of ~700 ppm; and (3) sample II-1(2)A has a water content of ~500 ppm. When moving toward the boundary between garnet amphibolite and gneiss, garnets exhibit an increase in water concentration. Both minerals from garnet amphibolite and gneiss have higher water contents than those from the eclogite. For omphacite, five samples of eclogite II-2A through II-5A have relatively homogeneous water contents of 1170 to 1485 ppm, whereas two samples of eclogite [II-1A and II-1(2)A] and one garnet amphibolite (II-6A) have significantly higher water contents of 4023 to 20745 ppm.

4.2.2. Hydrogen isotope

The H isotope compositions of garnet and omphacite from the two CCSD-MH segments are listed in Table 1 and illustrated in Figs. 5–8. Large variations in δD values from different samples are observed. For the first core segment, δD values for garnet and omphacite from the eclogites are −95‰ to −64‰ and −104‰ to −82‰, respectively; δD values for garnet from the gneisses range from −109‰ to −81‰. For the second core segment, δD values for garnet and omphacite from the eclogites range from −92‰ to −78‰ and −102‰ to −87‰, respectively; the garnet amphibolite has δD values of −116‰ for garnet and −89‰ for omphacite, respectively; garnet from gneiss has δD values of −110‰ to −105‰. It seems that the eclogite from both segments has similar hydrogen isotope compositions. This may indicate that their protolith has a similar geochemical nature and

Table 1
TC/EA-MS analyses of the hydrogen isotope composition and H_2O concentration of garnet and omphacite from two continuous core segments at different depths of CCSD-MH

Sample	Rock type	Garnet				Omphacite			$\Delta D_{Gt\text{-}Omp}$ (‰)
		Depth (m)	H content (ppm wt)	Total H_2O (ppm wt)	δD (‰)	H content (ppm wt)	Total H_2O (ppm wt)	δD (‰)	
First core segment									
02CCSD-I1A	Gneiss	737.16	107	963	−109				
02CCSD-I2A	Gneiss	736.93	104	936	−90				
02CCSD-I3A	Gneiss	736.74	78	702	−81				
02CCSD-I4A	Gneiss	736.46	89	801	−101				
02CCSD-I5A	Eclogite	736.28	139	1251	−92	667	6003	−95	3
02CCSD-I6A	Eclogite	736.01	134	1206	−95	586	5274	−98	3
02CCSD-I7A	Eclogite	735.87	92	828	−89	468	4212	−104	15
02CCSD-I8A	Eclogite	735.52	80	720	−78	187	1683	−83	5
02CCSD-I9A	Eclogite	735.37	74	666	−82	169	1521	−97	15
02CCSD-I10A	Eclogite	735.20	72	648	−64	203	1827	−94	30
02CCSD-I11A	Eclogite	735.02	81	729	−77	140	1260	−90	13
02CCSD-I12A	Eclogite	734.78	70	630	−64	167	1503	−82	18
02CCSD-I13A	Eclogite	734.39	83	747	−86	264	2376	−91	4
02CCSD-I14A	Eclogite	734.13	79	711	−74	206	1854	−88	14
Second core segment									
02CCSD-II1A	Eclogite	932.81	79	711	−81	1147	10323	−101	20
02CCSD-II1(2)A	Eclogite	932.49	58	522	−78	447	4023	−102	24
02CCSD-II2A	Eclogite	932.21	80	720	−80	165	1485	−92	12
02CCSD-II3A	Eclogite	932.03	104	936	−86	158	1422	−91	4
02CCSD-II4(1)A	Eclogite	931.74	98	882	−92	130	1170	−87	−6
02CCSD-II4(2)A	Eclogite	931.56	75	675	−85	147	1323	−90	5
02CCSD-II5A	Eclogite	931.33	77	693	−83	160	1440	−102	19
02CCSD-II6A	Amphibolite	931.11				2305	20745	−89	
02CCSD-II8A	Amphibolite	930.52	115	1035	−116				
02CCSD-II9A	Gneiss	930.32	176	1584	−110				
02CCSD-II12A	Gneiss	929.72	121	1089	−105				

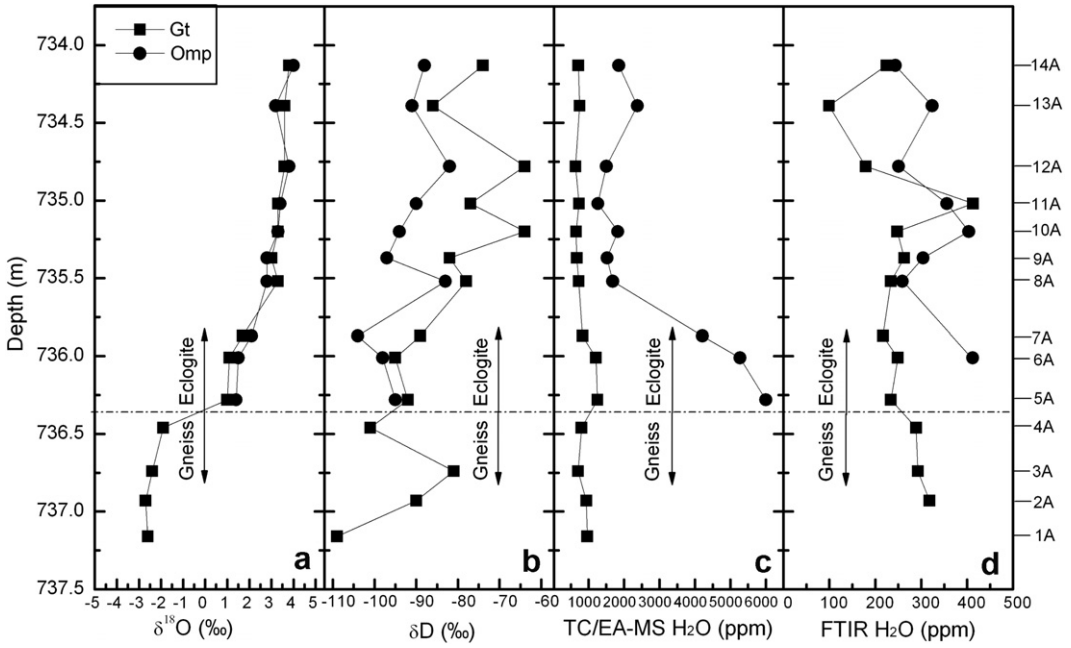

Fig. 5. Profiles of $\delta^{18}O$ values, δD values, water concentrations (in the forms of total H_2O and structural OH) in the first core segment (02CCSD-I). The O isotope profile is after Zhao et al. (2007).

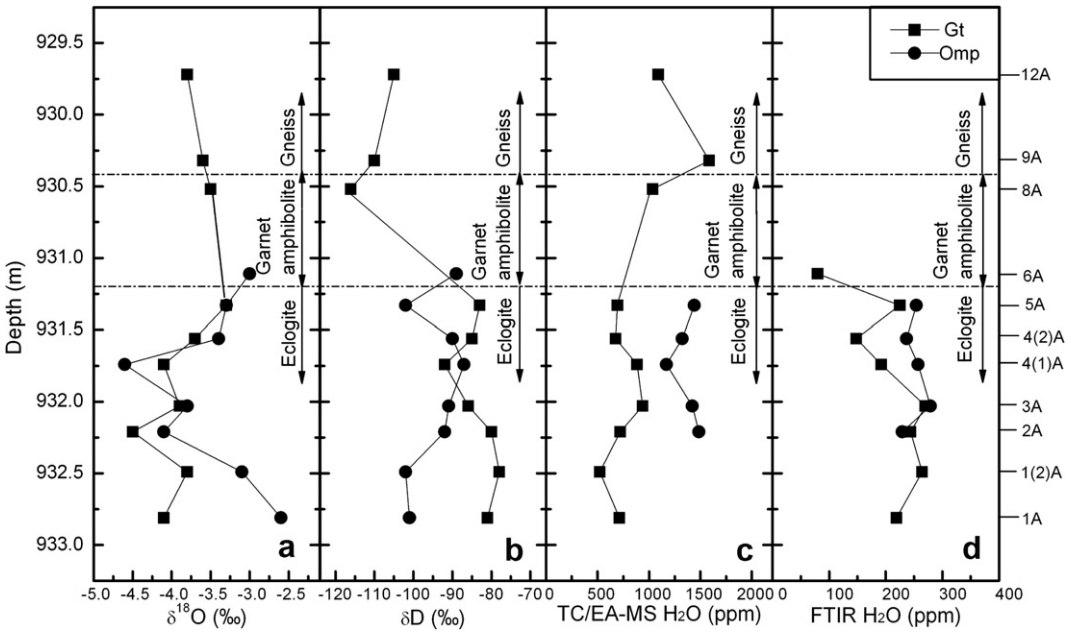

Fig. 6. Profiles of $\delta^{18}O$ values, δD values, water concentrations (in the forms of total H_2O and structural OH) in the second core segment (02CCSD-II). The O isotope profile is after Zhao et al. (2007).

underwent similar fluid processes during subduction and exhumation.

Figs. 5 and 6 show profiles of δD values for garnet and omphacite from the first and second core segment, respectively. For the first core segment, garnets from the eclogites away from the boundary between eclogite and gneiss have δD values higher than those close to the boundary, showing a progressive decrease in δD values toward the boundary. The gneiss I-1A has the lowest δD value of $-116‰$ for garnet, whereas garnets from the other samples of gneiss have δD values that are similar to those for eclogite close to the boundary (Figs. 5b and 8a). The δD values for omphacite show a trend that is similar to that for garnet, and they display δD values close to the contact that are lower than those

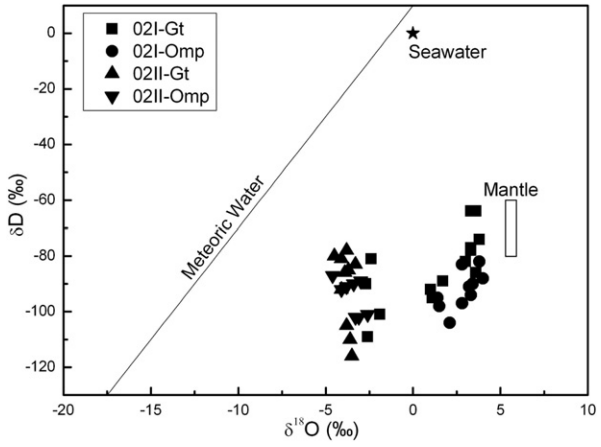

Fig. 7. Hydrogen and oxygen isotope compositions of garnet and omphacite from the two continuous CCSD-MH core segments (O isotope data from Zhao et al., 2007).

away from the contact (Figs. 5b and 8b). This indicates a progressive decrease in δD values toward the boundary.

For the second core segment, the eclogite has a small variation in δD values for garnet. When moving toward the boundary between eclogite and amphibolite, garnets exhibit a significant decrease in δD value. Eclogites II-1A through II-5A have δD values of $-92‰$ to $-78‰$ for garnet, whereas garnet amphibolite and gneiss have garnet δD values of $-116‰$ to $-105‰$. Four samples of eclogite II-2A through II-4(2)A and one sample of garnet amphibolite II-6A have relatively homogeneous δD values of $-92‰$ to $-87‰$ for omphacite, whereas those from the other samples have lower δD values of $-102‰$ to $-101‰$ for omphacite. Except for one eclogite [02-II4(1)A] with a negative H isotope fractionation of $-6‰$ between garnet and omphacite, all of the other samples of eclogite have positive fractionations of 3‰ to 30‰ between garnet and omphacite (Table 1).

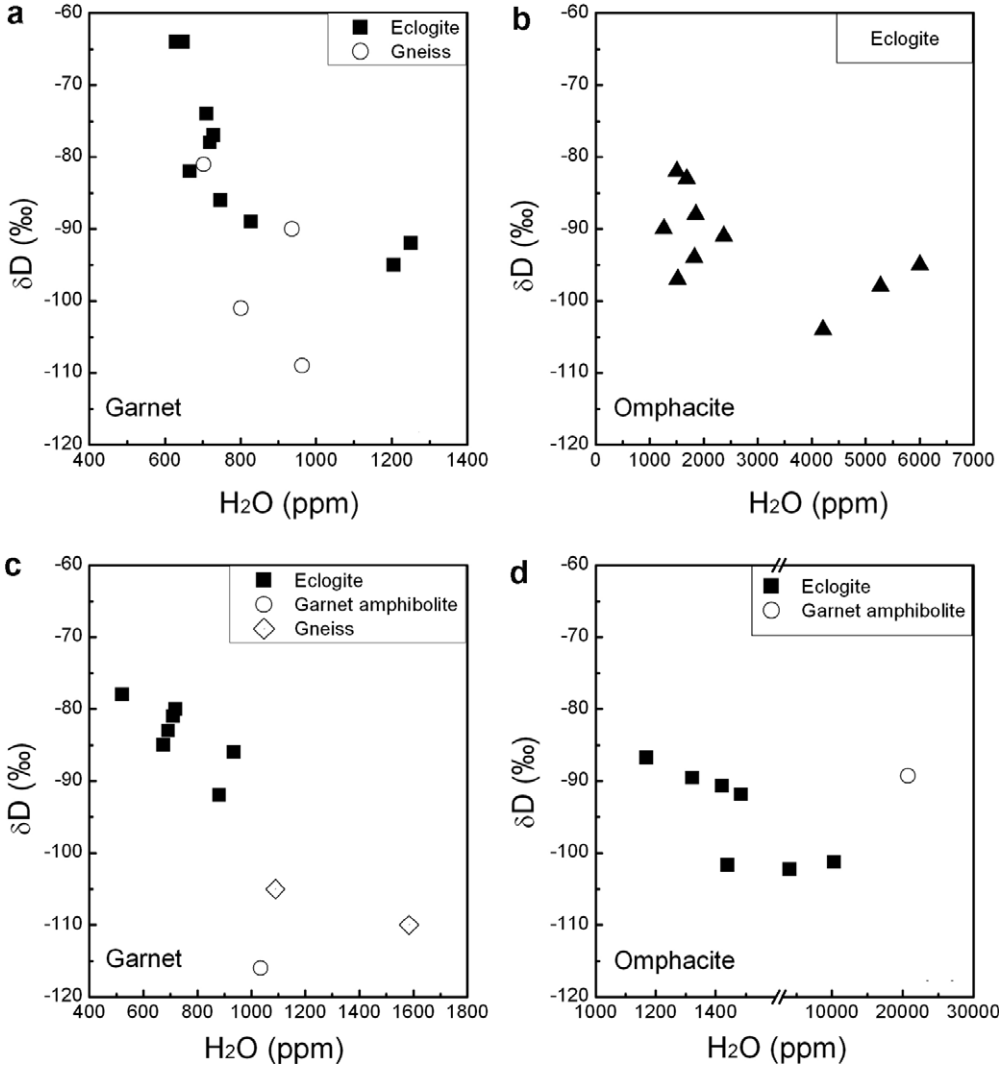

Fig. 8. Plot of total H_2O concentration vs. the hydrogen isotope composition of garnet and omphacite from the two continuous CCSD-MH core segments. (a) garnet from eclogite and gneiss in the first core segment (02CCSD-I); (b) omphacite from eclogite in the first core segment (02CCSD-I); (c) garnet from eclogite, garnet amphibolite and gneiss in the second core segment (02CCSD-II); (d) omphacite from eclogite and garnet amphibolite in the second core segment (02CCSD-II).

4.3. Structural water

4.3.1. Hydrogen species

All of the analyzed grains of garnet and omphacite from the two core segments exhibit several absorption bands in the typical OH-stretching vibration region (3000–3800 cm^{-1}), the representative unpolarized infrared spectra are illustrated in Fig. 9 and the detailed information is listed in Tables 2 and 3.

The OH-absorption bands of garnet can be divided into three groups: (I) 3620–3640 cm^{-1}; (II) 3560–3580 cm^{-1}; (III) 3400–3420 cm^{-1} (Fig. 9a and Table 2). Some spectra display a weak band at ~3730 cm^{-1}; it is probably created by subtraction of a background spectrum that was slightly contaminated by the presence of water vapor. These bands are similar to those found in Bixiling garnets (Xia et al., 2005). The position of group III bands is out of the previous investigated natural and synthesized garnets (Aines and Rossman, 1984a,b; Rossman and Aines, 1991; Rossman et al., 1989; Bell and Rossman, 1992b; Beran et al., 1993; Langer et al., 1993; Snyder et al., 1995; Lu and Keppler, 1997; Matsyuk et al., 1998; Withers et al., 1998; Zhang et al., 2001; Su et al., 2002). These bands are generally much broader than group I and II bands, with FWHH often larger than 180. They are typical of the stretching vibrations ($\upsilon_3 + \upsilon_1$) of molecular water. Therefore, this band is most likely due to the presence of molecular H_2O, such as submicroscopic fluid inclusions (e.g., Xia et al., 2005; Katayama et al., 2006). The shape and position of groups I and II bands are similar to the spectra of the hydrogrossular (Rossman and Aines, 1991) and hydroandradites (Amthauer and Rossman, 1998), which were ascribed to the presence of structural hydroxyl in the form of substitution $(SiO_4)^{4-} \leftrightarrow (O_4H_4)^{4-}$.

IR unpolarized spectra of omphacite showed three hydroxyl absorption bands in the region of 3440–3460 cm^{-1}(group I), 3500–3530 cm^{-1} (group II) and 3600–3625 cm^{-1} (group III) (Fig. 9b and Table 3). Generally, the group I band is typically the most intense and the group III band is the least intense in the spectrum. In some cases, group II is more intense. Some spectra of omphacite also display a weak band at ~3730 cm^{-1}; it is probably created by subtraction of a background spectrum that was slightly contaminated by the presence of water vapor. For the averaged spectra, the group I band is the most intense and the group III band is the least intense. The similar hydroxyl band positions were reported in both synthetic and natural clinopyroxenes, with relative band intensities depending on composition (Skogby et al., 1990; Smyth et al., 1991; Katayama and Nakashima, 2003; Bromiley and Keppler, 2004; Bromiley et al., 2004a; Katayama et al., 2006). For omphacitic pyroxene, the group I band is predominant in the spectrum with strong polarization of maximum absorption in the γ direction (Smyth et al., 1991). In our measurements, the relative absorbances of hydroxyl bands are variable for different grains of the same samples. This is attributed to different orientations of different grains with respect to the infrared beam direction. In order to overcome this variability, large numbers of grains (20–30) were measured and averaged for each sample following the protocol of Katayama et al. (2006).

4.3.2. Water content

In the region of 3000–3800 cm^{-1}, three group bands were fitted with Gaussian band shape after baseline correction, and their corresponding peak areas were obtained. For garnet, only the areas of groups I and II were used for calculation of structural water content. For omphacite,

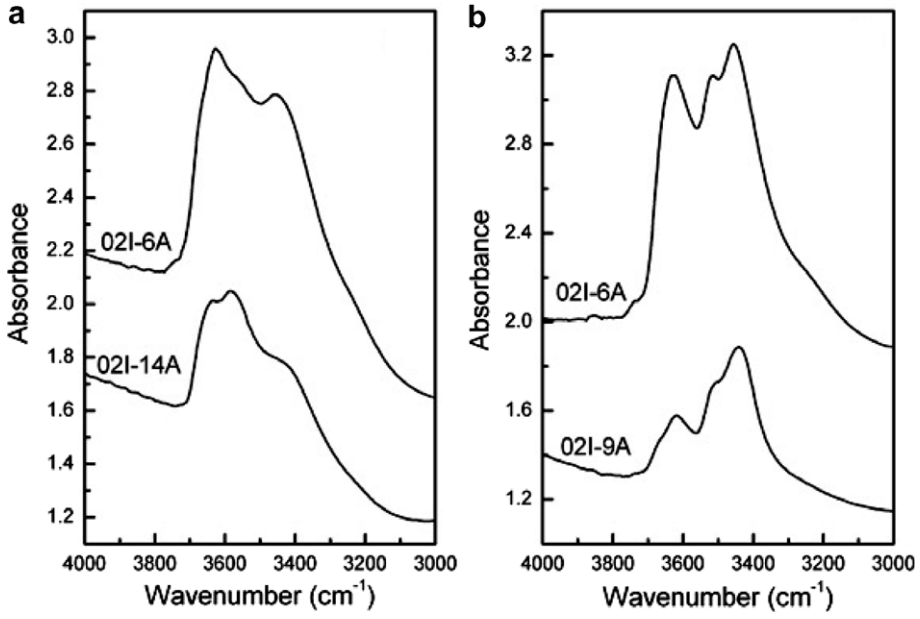

Fig. 9. Representative unpolarized infrared spectra of garnet (a) and omphacite (b) from CCSD-MH core samples. All the spectra were normalized to 1 mm thickness but were vertically offset.

Table 2
FTIR analysis of hydroxyl content in garnet from two core segments at different depths of CCSD-MH

Sample	Rock type	Depth (m)	Thickness (cm)	Group I (3620–3640 cm^{-1})			Group II (3560–3580 cm^{-1})			Group III (3400–3420 cm^{-1})			Structural OH (H_2O ppm wt)
				Intensity	FWHH	Area	Intensity	FWHH	Area	Intensity	FWHH	Area	
First core segment													
02I-2A	Gneiss	736.93	0.021	0.052	75	4.7	0.043	101	4.6	0.038	202	8.8	318
02I-3A	Gneiss	736.74	0.026	0.064	97	6.7	0.032	111	4.0	0.037	204	8.9	293
02I-4A	Gneiss	736.46	0.015	0.037	81	3.5	0.022	102	2.5	0.030	224	7.4	289
02I-5A	Eclogite	736.28	0.012	0.027	97	2.8	0.010	104	1.1	0.010	158	1.9	234
02I-6A	Eclogite	736.01	0.029	0.067	73	5.2	0.046	99	4.9	0.056	222	14.7	249
02I-7A	Eclogite	735.87	0.019	0.047	95	4.8	0.008	109	0.9	0.022	204	5.1	217
02I-8A	Eclogite	735.52	0.021	0.049	85	4.6	0.017	118	2.2	0.047	259	13.2	234
02I-9A	Eclogite	735.37	0.028	0.062	82	5.4	0.042	105	4.8	0.068	208	16.9	263
02I-10B	Eclogite	735.20	0.026	0.066	83	5.9	0.031	93	3.1	0.052	216	13.0	248
02I-11A	Eclogite	735.02	0.016	0.041	81	3.7	0.049	101	5.5	0.040	185	8.3	413
02I-12A	Eclogite	734.78	0.040	0.065	78	5.6	0.040	103	4.4	0.054	181	11.9	179
02I-13A	Eclogite	734.39	0.035	0.037	64	2.6	0.019	90	2.2	0.013	154	2.3	99
02I-14A	Eclogie	734.13	0.039	0.070	81	6.4	0.053	99	5.8	0.068	181	14.4	224
Second core segment													
02II-1A	Eclogite	932.81	0.018	0.041	63	2.9	0.023	99	2.6	0.013	156	2.4	219
02II-1(2)A	Eclogite	932.49	0.018	0.045	80	4.2	0.020	106	2.4	0.020	188	4.3	264
02II-2A	Eclogite	932.21	0.025	0.068	64	5.0	0.035	91	3.5	0.036	187	7.6	244
02II-3A	Eclogite	932.03	0.022	0.048	66	3.7	0.044	97	4.6	0.036	172	7.2	270
02II-4(1)A	Eclogite	931.74	0.019	0.035	64	3.1	0.018	95	2.0	0.020	178	4.4	192
02II-4(2)A	Eclogite	931.56	0.020	0.028	65	1.9	0.021	95	2.2	0.014	160	2.8	148
02II-5A	Eclogite	931.33	0.020	0.034	70	2.8	0.028	101	3.4	0.028	196	6.2	225
02II-6A	Garnet amphibolite	931.11	0.014	0.018	52	1.1	0.004	78	0.4	0.001	144	0.1	80

Table 3
FTIR analysis of hydroxyl content in omphacite from two core segments at different depths of CCSD-MH

Sample	Rock type	Depth (m)	Thickness (cm)	Group I (3440–3460 cm^{-1})			Group II (3500–3530 cm^{-1})			Group III (3600–3625 cm^{-1})			Structural OH (H_2O ppm wt)
				Intensity	FWHH	Area	Intensity	FWHH	Area	Intensity	FWHH	Area	
First core segment													
02I-6A	Eclogite	736.01	0.029	0.200	189	46.6	0.047	41	2.3	0.102	115	12.6	412
02I-8A	Eclogite	735.52	0.021	0.153	139	22.4	0.040	50	2.2	0.025	92	2.7	253
02I-9A	Eclogite	735.37	0.028	0.218	152	35.3	0.058	46	2.9	0.041	89	4.6	297
02I-10A	Eclogite	735.20	0.026	0.246	156	41.5	0.068	50	3.7	0.069	99	8.2	400
02I-11A	Eclogite	735.02	0.016	0.152	143	23.4	0.037	41	1.6	0.030	106	3.7	348
02I-12A	Eclogite	734.78	0.040	0.289	138	43.3	0.069	47	3.4	0.033	95	3.8	245
02I-13A	Eclogite	734.39	0.035	0.298	146	47.2	0.075	43	3.5	0.058	100	6.8	319
02I-14A	Eclogite	734.13	0.039	0.248	143	38.5	0.083	55	4.8	0.040	89	4.9	240
Second core segment													
02II-2A	Eclogite	932.21	0.025	0.116	162	19.3	0.060	48	3.3	0.061	92	6.7	228
02II-3A	Eclogite	932.03	0.022	0.174	139	25.1	0.065	40	2.8	0.031	96	3.6	278
02II-4(1)A	Eclogite	931.74	0.019	0.147	132	19.9	0.065	40	2.8	0.017	86	1.9	251
02II-4(2)A	Eclogite	931.56	0.020	0.139	128	18.8	0.066	38	2.7	0.024	94	2.8	236
02II-5A	Eclogite	931.33	0.020	0.149	134	20.7	0.060	38	2.4	0.021	91	2.5	248

after baseline correction, the area of all three obtained bands was used for water content calculation. Garnet is optically isotropic, but because of the heterogeneity between different grains of the same sample (Xia et al., 2005), the average of more than 15 grains was used to calculate the water content of each sample. For omphacite, because it is optically anisotropic, different grains may have different orientations with respect to the infrared beam direction. So we have attempted to overcome this variability by measuring large numbers of grains (20–30) and averaging the results.

Intrinsic hydroxyl contents (expressed as H_2O wt) in garnet and omphacite from the two core segments are listed in Tables 2 and 3, respectively. For the first core segment, the intrinsic hydroxyl contents of minerals from eclogite range from 99 to 413 ppm for garnet and 240 to 412 ppm for omphacite, respectively; whereas the garnets from the gneiss have water contents of 289–318 ppm. For the second core segment, the water content of minerals are 80–270 ppm for garnet, and 228–278 ppm for omphacite, respectively. It appears that the water content of omphacite is variably higher than that of garnet, indicating that water prefers to dissolve into omphacite rather than garnet in eclogite.

The profile of intrinsic hydroxyl contents in garnet from the eclogites, gneisses and garnet amphibolite as well as in omphacite from the eclogites are plotted in Figs. 5d and 6d for the two core segments. For the first core segment, six samples of eclogites I-5A through I-10A that are close to the eclogite–gneiss boundary and one sample away from the boundary have relatively homogeneous garnet water contents of 217–263 ppm, within the analytical uncertainties. However, eclogite I-11A has the highest water content of 413 ppm for garnet, whereas the samples I-13A and I-12A have the lowest water contents of 99–179 ppm in garnet (Table 2 and Fig. 5d). The water contents in garnet from the gneisses are slightly higher than those from the eclogites, with the exception of sample I-11A (Fig. 5d).

For the second core segment, four samples of eclogites, II-1A through II-3A, away from the boundary between eclogite and garnet amphibolite and one sample close to the boundary have relatively homogeneous water contents of 219–270 ppm in garnet, within the analytical uncertainties. However, eclogites II-4(1)A and II-4(2)A have slightly lower water contents of 192 and 148 ppm in garnet than do the others (Table 2 and Fig. 6d). Because garnet in the gneisses is rare and fine-grained, its water content was not able to be measured. Similarly, only one garnet amphibolite was measured for its water content in garnet. Nevertheless, the measured garnet amphibolite has the lowest water content of 80 ppm in garnet.

Difficulties were also encountered in the FTIR analysis of the water content of omphacite in some eclogites from the two core segments. Because of the retrograde metamorphism of the largest degree, samples I-5A and I-7A from the first core segment and samples II-1A and II-1(2)A from the second core segment were not able to be measured for water content in omphacite. Nevertheless, the available data are enough to show water content variation with spatial distribution for omphacite from the two core segments (Figs. 5d and 6d). For the first core segment, three samples of eclog-

ite I-12A through I-14A away from the eclogite–gneiss boundary as well as samples I-8A and I-9A have relatively homogeneous omphacite water contents of 240–319 ppm, within the analytical uncertainties (Table 3 and Fig. 5d), whereas two samples of eclogite I-11A and I-10A in the midst of the eclogites and one sample I-6A close to the boundary between eclogite and gneiss have slightly higher water contents of 348–412 ppm in omphacite. For the second core segment, the eclogites have homogeneous omphacite water contents of 228–278 ppm, within the analytical uncertainties (Table 3 and Fig. 6d).

5. DISCUSSION

5.1. Stable isotope variation and fractionation

A large variation in $\delta^{18}O$ from $-11‰$ to $10‰$ have been observed in the UHP eclogites and associated gneisses from the surface outcrops along the Dabie-Sulu orogenic belt, with both equilibrium and disequilibrium fractionations of O isotopes between coexisting minerals (Zheng et al., 2003; and references therein). The consensus is that the UHP rocks acquired their unusually negative $\delta^{18}O$ values, down to $-11‰$, by high-T meteoric-hydrothermal alteration during the middle Neoproterozoic period (Rumble et al., 2002; Zheng et al., 2004) which was a long time before the Triassic UHP metamorphism. A detailed O isotope study has been carried out by Zhao et al. (2007) for the two CCSD-MH core segments. As illustrated in Figs. 5a, 6a and 7, the eclogites and gneisses from the two core segments show variable ^{18}O-depletion relative to the normal mantle-derived rocks ($\delta^{18}O = 5.7 \pm 0.3‰$). The ^{18}O-depletion in the two core segments is also ascribable to the hydrothermal alteration of their protoliths by meteoric water at elevated temperatures before the continental subduction.

The present study shows that most of the samples from the two core segments have δD values of $-116‰$ to $-64‰$ for garnet and $-104‰$ to $-82‰$ for omphacite (Table 1 and Fig. 7). They are comparable with δD values of $-127‰$ to $-83‰$ for phengite, $-93‰$ to $-81‰$ for amphibole and $-66‰$ to $-49‰$ for epidote from eclogite and quartz schist from outcrops surrounding CCSD-MH in the Donghai area (Rumble and Yui, 1998; Zheng et al., 1998). Our new data confirm the previous conclusion that the stable isotope signatures of meteoric water were incorporated into the protoliths of UHP eclogites and associated gneisses by high-T hydrothermal alteration and subsequent magmatism (Rumble and Yui, 1998; Zheng et al., 1998, 2003).

In the transition between eclogite and gneiss from the first core segment (Fig. 5a), the gradual decrease occurs in eclogite $\delta^{18}O$ when moving towards the gneiss, but with a stepped increase at the boundary. The O isotope study of Zhao et al. (2007) has demonstrated that the observed heterogeneity in $\delta^{18}O$ is attributable to the differences in protolith $\delta^{18}O$ and such changes in the contact suggest an enhanced water–rock interaction during magma emplacement of gneiss protolith. The profile of mineral H isotopes from the first eclogite core segment shows a similar trend to that of O isotopes; a decrease in heavy isotope content towards the boundary is observed (Fig. 5b). Therefore, the observed variation in the H isotope profile is, to some extent, attributed to the differences in protolith δD.

As shown by Fig. 4, the degree of retrograde metamorphism generally increases with decreasing distance from the eclogite–gneiss boundary. The eclogites from the two core segments exhibit different degrees of retrograde metamorphism, and more abundant symplectites were observed in the contacts between eclogite and gneiss. This is especially profound for the eclogites in the second core segment, as indicated by a transitional zone of garnet amphibolite between eclogite and gneiss. In the garnet amphibolite, most omphacites were retrograded to symplectite with few relict garnets, but amphibole and biotite become abundant. This indicates that the eclogite is significantly retrograded to garnet amphibolite or eclogitic gneiss at the contact between contrasting lithologies during exhumation due to the difference in fluid content (e.g., Zhang et al., 2003). Therefore, isotopic exchange would occur between minerals and retrograde fluid during exhumation, which may change the H isotope composition of minerals and thus, may alter the H isotope fractionations between different minerals.

Except for a negative H isotope fractionation of $-6‰$ between garnet and omphacite from one sample of eclogite, all of the other samples of eclogite show positive fractionations of $3‰$ to $30‰$ between the two minerals (Table 1). Positive D/H fractionations for the total water between garnet and omphacite are also observed from outcrop eclogites at Bixiling in the Dabie orogen (Gong et al., 2007a) and at Taohang in the Sulu orogen (Gong et al., 2007b). Although no experimental data is available for equilibrium D/H fractionations between omphacite and garnet at high temperatures, $\Delta D_{\text{Garnet–Augite}} = 2‰$ and $\Delta D_{\text{Garnet–Othopyroxene}} = 10‰$ were proposed by Bell and Ihinger (2000) based on differences in OH stretching frequency between these minerals from mantle-derived xenoliths. Because omphacite has similar OH stretching frequencies to those of augite and orthopyroxene, H isotope fractionation between garnet and omphacite should be similar to that between garnet and augite. Nevertheless, the D/H fractionations between garnet and pyroxene proposed by Bell and Ihinger (2000) were for structural water in the nominally anhydrous minerals. For our case, however, the H isotope compositions of garnet and omphacite determined by TC/EA-MS were for total water in the minerals. This total water contains all hydrous phases present in the minerals, including both molecular water (e.g., fluid inclusions and hydrous phase inclusions) and structural hydroxyl. Stepwise-heating TC/EA-MS analyses for a garnet from UHP eclogite at Bixiling in the Dabie orogen show that the total water and molecular H_2O are depleted in D relative to structural hydroxyl. In this regard, it is reasonable to expect that the equilibrium D/H fractionation in total water between garnet and omphacite is still positive and larger than that of structural hydroxyl. Therefore, both equilibrium and disequilibrium fractionations occur between garnet and omphacite from the two CCSD-MH core segments.

For the first CCSD-MH core segment, half of the eclogites have $\Delta D_{\text{Garnet–Omphacite}}$ values of about $14‰$ (Table 1 and Fig. 10a), which might be the equilibrium fractionation between garnet and omphacite at eclogite-facies conditions. As discussed above, the eclogites have principally preserved

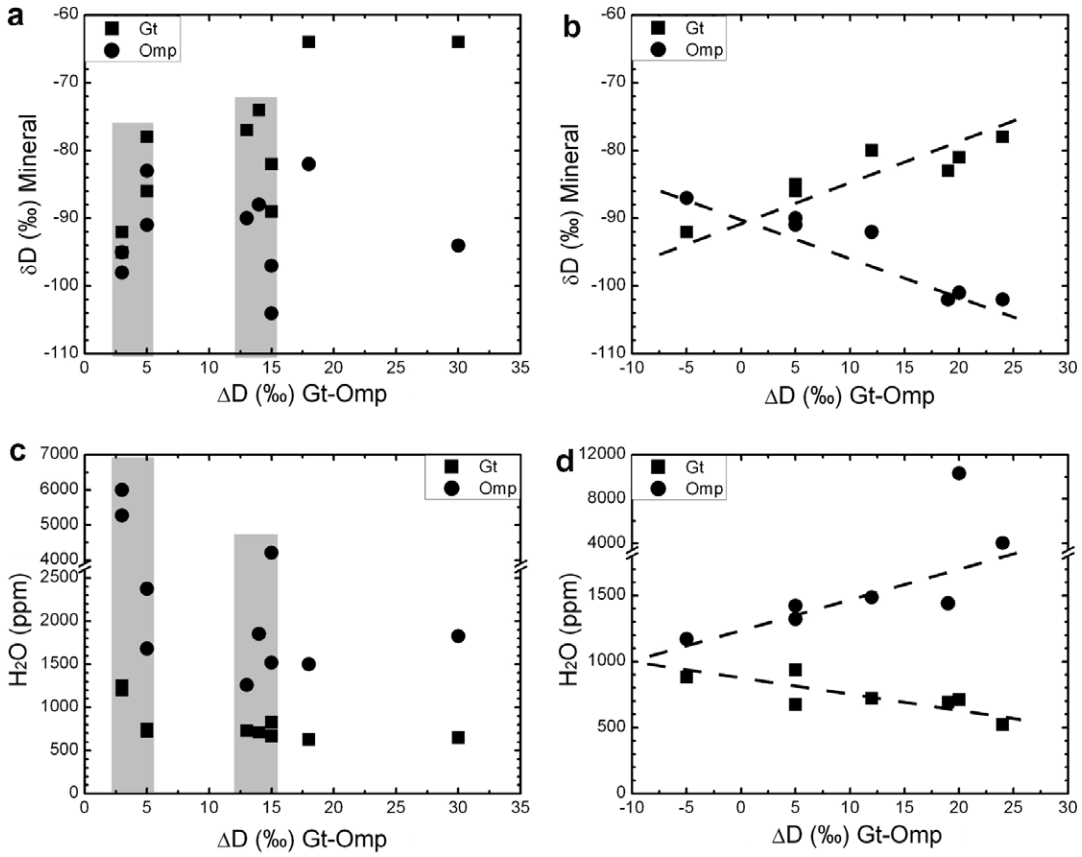

Fig. 10. Plots of H isotope fractionations between garnet and omphacite vs. either δD values or total water content for garnet and omphacite from the two continuous CCSD-MH core segments. (a) mineral δD vs. $\Delta D_{\text{Gt-Omp}}$ for the first core segment (02CCSD-I); (b) mineral δD vs. $\Delta D_{\text{Gt-Omp}}$ for the second core segment (02CCSD-II); (c) mineral H_2O content vs. $\Delta D_{\text{Gt-Omp}}$ for the first core segment (02CCSD-I); (d) mineral H_2O content vs. $\Delta D_{\text{Gt-Omp}}$ for the second core segment (02CCSD-II).

the H isotope feature of their protoliths. Eclogite I-9A through I-14A away from the contact between eclogite and gneiss, especially I-9A, are less retrograded compared with those close to the eclogite–gneiss boundary. Thus, they might have preserved the equilibrium H isotope fractionation between garnet and omphacite acquired during the eclogite-facies metamorphism. As shown by Fig. 5b, much smaller fractionations between garnet and omphacite with a value of about 4‰ occur in two δD-decreased samples of eclogite I-5A and I-6A close to the boundary as well as two samples of eclogite I-8A and I-13A away from the boundary (Table 1 and Fig. 10a). This indicates that the H isotope composition of these samples was reset by retrograde metamorphism and approached a new equilibrium (re-equilibrium) at amphibolite-facies conditions. While the two clusters of fractionation values at ~4‰ and ~14‰ are interpreted as being a response to different metamorphic conditions, it remains to be resolved whether there is a difference in water content between the two forms of water in the two eclogite minerals.

For the second core segment, except for sample II-4(1)A, the δD values for omphacite are lower than those for garnet (Fig. 6b). Garnet δD values tend to increase with an increasing difference in δD between garnet and omphacite, whereas omphacite δD values tend to decrease (Fig. 10b). As a result, H isotope fractionations between garnet and omphacite vary regularly with the δD values for individual minerals. Apparently, the H isotope fractionation behavior of the two minerals contrasts during metamorphism. Because there are more than two phases in the studied system for representing mass conservation in δ–Δ space, no simple geochemical meaning can be derived from the intercept and slopes of correlation arrays on the δ–Δ diagram (Zheng, 1992). Therefore, the contrasting correlation arrays in Fig. 10b may indicate H isotope exchange between garnet and omphacite in a relatively closed system. Experimental studies of H diffusion in nominally anhydrous minerals suggest that the rate of H diffusion in garnet is much slower than that in omphacite (Ingrin et al., 1995; Wang et al., 1996; Ingrin and Skogby, 2000; Stalder and Skogby, 2003; Blanchard and Ingrin, 2004a,b; Zhao and Zheng, 2007). Therefore, the contrasting fractionation behavior of H isotopes in the two minerals is caused by differential exchange of H isotopes with retrograde fluid during exhumation. The similar behaviors of differential H isotope exchange were also observed for hydrous minerals from UHP eclogites and gneiss in the Dabie-Sulu orogenic belt (Zheng et al., 1998, 1999; Fu et al., 1999). Furthermore, it was observed that two samples II3A and II4(2)A have H isotope fractionations of about 4‰ which are similar to those from the first core segment. The other samples from the second core segment are also converging towards that value. This may point

to H isotope re-equilibration between the structural hydroxyl groups of garnet and omphacite due to isotopic resetting during amphibolite-facies retrogression.

As shown by Fig. 5a, eclogite I-8A through I-14A away from the boundary between eclogite and gneiss have relatively homogeneous $\delta^{18}O$ values, whereas the δD values for the same samples show a large variation and thus, indicate a large scatter in the H isotope fractionation between garnet and omphacite (Fig. 5b). Also, the H isotope fractionations between garnet and omphacite were re-equilibrated by amphibolite-facies retrogression for the samples close to the contact between eclogite and gneiss. In contrast, the O isotope fractionations have preserved the equilibrium values acquired during the eclogite-facies metamorphism without significant influence by the amphibolite-facies retrogression. These indicate that the H isotope compositions of garnet and omphacite are more susceptible to retrograde exchange than the O isotopes in the two minerals. Experimental studies have shown that the rate of H isotope exchange between hydrous minerals and water is much faster than O isotope exchange in the same system (Freer, 1981; Farver and Gilletti, 1985; Fortier and Gilletti, 1989, 1991; Zheng and Fu, 1998; Zhao and Zheng, 2007). It is possible that water in nominally anhydrous minerals may isotopically behave like that in hydrous minerals during high-T geochemical processes and thus, that the rate of H isotope exchange between nominally anhydrous minerals and water is much faster than O isotope exchange. Therefore, the different isotopic behaviors between H and O isotopes for garnet and omphacite are caused by differential exchange of H and O isotopes with retrograde fluid during exhumation (Zheng et al., 2003).

As shown by Fig. 8, garnet and omphacite from the two core segments show a roughly negative correlation between δD values and total water contents. This covariation can be explained by preferential loss of H-rich fluid relative to D-rich fluid from the minerals during exhumation. The similar H_2O-δD negative correlation was also found in clinopyroxene megacryst and ascribed to diffusive H loss during magma ascent to the surface (e.g., Newman et al., 1988). While in principle the H-rich fluid diffuses much faster than the D-rich fluid, it is more possible that molecular H_2O diffuses faster than the structural OH (e.g., Zhang et al., 1991; Doremus, 2004). Thus, the observed H isotope variations in the two CCSD-MH core segments may be principally caused by the preferential loss of molecular H_2O from garnet and omphacite during the exhumation of deeply subducted continental crust. Furthermore, the total water content in garnet and omphacite from the second core segment varies regularly with the H isotope fractionations between garnet and omphacite (Fig. 10d). This indicates that the loss of molecular H_2O is associated not only with preferred removal of hydrogen relative to deuterium, but also with concurrent H isotope exchange between garnet and omphacite. For the first core segment, in contrast, there is no substantial correlation between garnet and omphacite H isotope fractionation and total water content (Fig. 10c). This suggests that the H isotope exchange in this core segment occurred in open systems with the influence by aqueous fluid from the surrounding gneiss.

Both equilibrium and re-equilibrium H fractionations are observed between garnet and omphacite for the eclogites away from the boundary between eclogite and gneiss from the first core segment (Fig. 10a). The garnet and omphacite for these samples have homogeneous total water contents (Fig. 5c), whereas the hydroxyl contents of garnet and omphacite show considerable variations at the local scale (Fig. 5d). For the second core segment (Fig. 10b), the regular H isotope fractionations between garnet and omphacite suggest that their H isotope exchange occurs in a relatively closed system, possibly with the exsolved water serving as an exchange medium. In either case, the retrograde fluid was internally buffered in stable isotopic compositions as previously suggested by Zheng et al. (1999, 2003). Thus, the hydration of the eclogites away from the boundary between eclogite and gneiss could be caused by fluid that was locally derived from the eclogites themselves by the decompression exsolution of structural hydroxyl and molecular water during exhumation.

5.2. Mineral water contents and implications for the origin of retrograde fluid

It has been postulated that the retrograde fluid in UHP metamorphic rocks can be derived from the decomposition of hydrous minerals, the decrepitation of primary fluid inclusions, and the exsolution of structural hydroxyls from nominally anhydrous minerals during exhumation (Zheng et al., 2003). Minor amounts of hydrous minerals, such as phengite, zoisite/epidote, glaucophane and talc, have been observed to occur in some of the UHP metamorphic rocks from the Dabie-Sulu orogenic belt (e.g., Liou et al., 1995; Zhang et al., 1995, 2000, 2002), implying that they may still be stable at UHP conditions and therefore could store significant amounts of water inherited from premetamorphic protoliths. In the process of UHP slab exhumation, however, the hydrous minerals would decompose to provide a considerable amount of retrograde fluid (e.g., Miller et al., 2002; Schmidt and Poli, 2003; Zheng et al., 2003; Li et al., 2004). Intensive studies of fluid inclusions in minerals from Dabie-Sulu UHP eclogites show the preservation of prograde and peak metamorphic fluids despite significant disturbance during exhumation (e.g., Xiao et al., 2000, 2001, 2002; Fu et al., 2001, 2002, 2003a,b; Su et al., 2002). An abrupt decrease in pressure may cause decrepitation of fluid inclusion, producing small amounts of retrograde fluid (Zheng et al., 2003).

Furthermore, nominally anhydrous minerals, such as omphacite, garnet and rutile, may release water for hydration and symplectization during retrograde metamorphism of the UHP rocks (Zheng et al., 1999, 2003). It is well known that pyroxene, garnet and rutile in eclogites can contain a considerable amount of water in the form of OH in their crystal structures (Smyth et al., 1991; Bell and Rossman, 1992a; Rossman, 1996; Ingrin and Skogby, 2000; Bolfan-Casanova, 2005). Previous FTIR studies on nominally anhydrous minerals in the Dabie-Sulu UHP eclogites show that they contain significant amounts of hydroxyl, about 115–1300 ppm in omphacite and 92–1735 ppm in garnet (Zhang et al., 2001, 2004; Xia et al., 2005).

Both TC/EA-MS and FTIR analyses in this study have detected significant amounts of water in the forms of molecular H_2O and structural OH in garnet and omphacite from the UHP eclogite and gneiss from the two continuous CCSD-MH core segments. The total H_2O concentration determined by TC/EA-MS is 522–1584 ppm in garnet and 1170–20745 ppm in omphacite (Table 1). More water is present in omphacite than garnet from the eclogite (Figs. 5c and 6c). Garnet from the gneiss contains more water than that from the eclogite (Fig. 8a and c). The water distribution in the two continuous core segments is heterogeneous, as some have significantly higher water content than others. On the other hand, the hydroxyl contents detected by FTIR are 80–413 ppm in garnet and 228–412 ppm in omphacite (Tables 2 and 3). As shown by Fig. 11, the water contents as determined by TC/EA-MS are much higher than those determined by FTIR for the same samples. This is because the water concentrations determined by TC/EA-MS are for the total water, whereas those determined by FTIR only for the structural hydroxyl. It appears that the UHP metamorphic minerals contain much higher amounts of water in the forms of molecular H_2O and interstitial hydrous minerals than the intrinsic water in the form of structural hydroxyl, pointing to enhanced capacity of water storage in the UHP eclogite minerals. Nevertheless, omphacite still has slightly higher contents of structural hydroxyl than garnet from the eclogite (Figs. 5d and 6d). Garnet from the gneiss has slightly higher contents of the structural water than those from the eclogite (Fig. 5d).

The higher total water concentrations are found in garnet from the gneiss than from the eclogite in both core segments (Figs. 5c and 6c). Because the presence of water favors phase transition from coesite to quartz during exhumation, this explains the common observations that no UHP index mineral can be found in garnet from Dabie-Sulu UHP granitic orthogneisses (Wang et al., 1995; Cong, 1996; Liou et al., 1996). Generally, the gneisses have more water contents than the eclogites as they contain a lot of hydrous minerals, such as epidote, muscovite and biotite. This difference in total water content for garnet may be caused by the difference in the water content of their protolith. The three samples of eclogite (I-5A, I-6A and I-7A), close to the boundary between eclogite and gneiss, have the highest water contents in garnet. This may be ascribed to two possible causes: (1) inherited high water contents from the garnets formed during prograde UHP metamorphic conditions, or (2) water incorporated into garnet during retrograde HP metamorphism. In either case, the high water contents of the gneiss may be due to the high water contents of its protolith. On the contrary, the higher water contents in omphacite for the three eclogite samples close to the boundary may be due to incorporation of water into omphacite during retrograde metamorphism. As shown by Fig. 4, most of the omphacites are retrograded to symplectite in these samples.

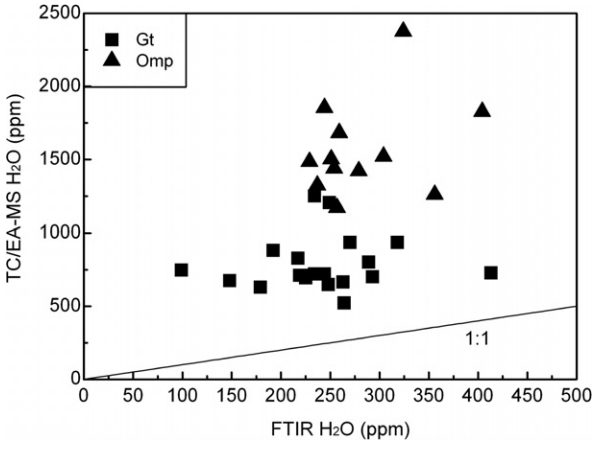

Fig. 11. Water contents by TC/EA-MS vs. those by FTIR for garnet and omphacite in eclogites and gneisses from the two CCSD-MH core segments.

With subduction of continental crust into mantle depths, water could be incorporated as both structural OH and molecular H_2O into nominally anhydrous minerals (e.g., omphacite, garnet and rutile) and hydrous minerals (e.g., phengite). During UHP metamorphism, the water is stable in both types of mineral. A number of experimental investigations have shown that hydroxyl solubility in nominally anhydrous minerals decreases with decreasing pressure (Lu and Keppler, 1997; Withers et al., 1998; Mosenfelder, 2000; Rauch and Keppler, 2002; Koch-Muller et al., 2003; Bromiley et al., 2004a,b; Mierdel and Keppler, 2004). A linear increase in the water content of omphacite and garnet with pressure was observed from the Kokchetav UHP eclogite (Katayama and Nakashima, 2003; Katayama et al., 2006). Thus, as previously suggested by Zheng et al. (1999, 2003), the solubility of hydroxyl in nominally anhydrous minerals decreases rapidly due to an abrupt decrease in pressure in the early stage of UHP slab exhumation, resulting in the release of significant amounts of aqueous fluid. In this regard, many of the nominally anhydrous minerals have lost significant amounts of their original water during the decompression upon ascent to crustal levels. Therefore, the above measured amounts of structural hydroxyl are only the minimum estimates of actual dissolved water in the nominally anhydrous minerals at mantle depths.

The heterogeneous hydroxyl contents in garnet and omphacite may be ascribed to four possible causes: (1) chemical differences that may influence H incorporation and diffusion; (2) different extents of hydroxyl exsolution from the host mineral in response to decompression during exhumation; (3) different degrees of reaction with exotic fluid during retrograde metamorphism; and (4) inherited heterogeneous water contents from minerals that formed/equilibrated during prograde metamorphic conditions. Since the rates of H diffusion in garnet and omphacite are very fast (Zhao and Zheng, 2007), the reaction between minerals and exotic fluid could result in an increase of hydroxyl water content in garnet and omphacite.

Despite the different extents of retrograde metamorphism, the six samples of eclogite I-5A through I-10A adjacent to the gneiss and one sample, I-14A, away from the gneiss have homogeneous hydroxyl contents of 217–263 ppm for garnet within the FTIR analytical uncertainties.

Thus, this may reflect water contents from the garnets that were formed/equilibrated during prograde UHP metamorphism. The higher hydroxyl content for eclogite I-11A may be caused by water incorporation into garnet during retrograde metamorphism, whereas the lower hydroxyl contents for eclogites I-12A and I-13A may be due to water loss during exhumation or to the low water content of their protolith. The hydroxyl contents of garnet from the eclogites in the second core segment are similar to those from the first core segment. The higher and relatively homogeneous water contents of 219–270 ppm may indicate water incorporation into garnet during prograde metamorphism. The lower hydroxyl contents of garnet from samples II-4(1)A and II-4(2)A may be due to water loss during exhumation or to the low water content of protolith. Compared to the eclogites, the gneisses have higher hydroxyl contents in garnet. This is concordant with the result from the TC/EA-MS analyses, reinforcing the expectation that the gneisses have more water than the eclogites.

For omphacite, three samples of eclogite I-12A through I-14A away from the eclogite–gneiss boundary as well as two eclogite, I-8A and I-9A, have relatively homogeneous omphacite water contents of 240–319 ppm, within the FTIR analytical uncertainties. These samples were less retrograded, such that the hydroxyl contents may reflect the water contents of omphacites that were formed/equilibrated during prograde UHP metamorphism. On the other hand, eclogite I-6A, I-10A and I-11A, which show larger extents of retrograde metamorphism, seem to have higher hydroxyl contents, indicating water incorporation into omphacite during retrograde HP metamorphism. For the second core segment, despite different extents of retrograde metamorphism, the eclogites show homogeneous hydroxyl contents in omphacite, indicating that the hydroxyl contents may reflect the water content of omphacites that were formed/equilibrated during prograde UHP metamorphism.

As discussed above, the eclogites adjacent to the gneiss from the first core segment show the H isotope re-equilibrium fractionations between garnet and omphacite, with the garnet δD values being similar to those of the gneiss. For the second core segment, the garnet amphibolite has similar δD values for garnet relative to those for the gneisses, but they were much lower than those from the eclogites away from the boundary between eclogite and gneiss. Both FTIR and TC/EA-MS analyses for the two core segments show that the gneisses have higher water contents of garnet than the eclogites. In addition, the hydrous minerals are still present in the gneiss, suggesting higher contents of water in the gneiss than in the eclogite. Thus, the retrograde fluids for the eclogites adjacent to the gneisses may mainly come from the gneiss. However, the occurrence of H isotope re-equilibrium fractionations between garnet and omphacite indicates that the fluid mobility is limited and thus is internally buffered in stable isotope composition. Also, the scale of fluid flow is limited because the samples away from the boundary between eclogite and gneiss do not seem to be influenced by the retrograde fluid from the gneisses. In this study, we can estimate that this length is not larger than 1 m. Furthermore, heterogeneity in mineral δD value and structural OH content is evident on scales of tens of centimeters between the different and same rock types (Figs. 5 and 6). This may correspond to the maximum scales of fluid flow during the continental collision.

5.3. Quantitative estimates of water loss from minerals during exhumation

With the deep subduction of continental crust, basaltic rocks were transformed to HP or UHP eclogite. This creates a lithology that is rich in clinopyroxene and garnet with a significant capacity for storing water as structural OH in nominally anhydrous minerals. Hauri et al. (2006) estimated the maximum H_2O content of nominally anhydrous eclogite, calculated along the P–T path of the water-saturated eclogite solidus of Schmidt and Poli (1998). Their calculations assumed a mineral assemblage of 65:25:10 clinopyroxene–plagioclase–olivine up to 1.5 GPa, transitioning to a 80:20 clinopyroxene/garnet mineralogy at 2 GPa persisting to 5 GPa, then gradually shifting to a 20:80 clinopyroxene–garnet mineralogy at 13.5 GPa as the stability field of garnet expands. They calculate the H_2O storage capacity for nominally anhydrous eclogite throughout the upper mantle by the used of these modal abundances, with estimates of the tetrahedral Al content of eclogitic pyroxenes derived from high pressure eclogite studies (Schmidt and Poli, 1998; Pertermann and Hirschmann, 2003; Aoki and Takahashi, 2004; Okamoto and Maruyama, 2004). The results show that the ability of nominally anhydrous eclogite to store water is greatest in the 2–4 GPa pressure interval (4000–5000 ppm H_2O) due to the presence of aluminous clinopyroxene as the dominant mineral phase. At pressures greater than 3 GPa, however, the stability field of garnet slowly expands at the expense of clinopyroxene, and the Al_2O_3 content of clinopyroxene diminishes slightly. The storage capacity of eclogite is correspondingly reduced by these changes in crystal chemistry and phase proportions, with a turnover of the H_2O storage capacity at a given pressure from 3 to 4 GPa (Hauri et al., 2006). Either the decrease in the Al_2O_3 content of clinopyroxene at high pressure or the presence of more garnet in eclogite can result in a decrease in the H_2O storage capacity of nominally anhydrous eclogite from 100 to 410 km depth.

Fluid availability from UHP eclogite itself depends on the persistent feature of the eclogite H_2O storage capacity with depth, varying little with slab P–T path and mainly being dominated by the Al_2O_3 content and proportion of clinopyroxene. It is expected with the prograde subduction prior to the diamond stability field that more and more hydroxyls would be dissolved into eclogite, possibly up to the maximum H_2O contents of 4000–5000 ppm (Hauri et al., 2006). With a further increase in pressure from the coesite to diamond stability field, however, the hydroxyl solubility would become decreased according to the estimate of Hauri et al. (2006). Hydroxyl exsolution is expected to take place at this stage, resulting in fluid availability for the first episodic growth of metamorphic zircon at 242 ± 2 Ma for the Dabie-Sulu UHP metamorphic rocks (Wu et al., 2006). In this regard, the pressure climax during the deep subduction would occur subsequent to, but close to, 242 ± 2 Ma. During the initial exhumation, on the other

hand, the pressure decrease also causes a significant decrease in the H_2O storage capacity of UHP eclogite. One-thousand to two-thousand parts per million H_2O could be released from nominally anhydrous minerals during the pressure transition from the diamond to coesite stability fields (Hauri et al., 2006). This brings about fluid availability for the second episodic growth of metamorphic zircon at 227 ± 2 Ma for the Dabie-Sulu UHP rocks (Wu et al., 2006). Continuous exsolution of hydroxyl from the nominally anhydrous minerals during the exhumation from UHP to HP eclogite-facies may be the basic reason why a large number of zircon U–Pb ages from 225 to 210 Ma have been dated for the Dabie-Sulu UHP rocks (e.g., Ames et al., 1996; Hacker et al., 1998, 2000; Li et al., 2004; Liu and Xu, 2004; Liu et al., 2004a,b; Wan et al., 2005; Zheng et al., 2005b; Zhao et al., 2006).

Due to the decompression effect, many nominally anhydrous minerals have lost significant portions of their original water during exhumation (Fig. 12). In order to estimate the amount of water lost from eclogite by the decompression exsolution of structural hydroxyl, we need to know the initial water content prior to dehydration, the remaining water content subsequent to dehydration, and the densities of garnet and omphacite in UHP eclogites. The parameters used in the present calculations were determined in the following ways.

(1) *Initial water content*. Structural hydroxyl contents in garnets from Dabie-Sulu UHP eclogites range from 92 to 1735 ppm H_2O (Zhang et al., 2004; Xia et al., 2005). Garnet in this study has structural hydroxyl contents in the range of 99–413 ppm. The total water contents in garnet from the CCSD-MH eclogites are 522–1251 ppm, such that the initial hydroxyl content in garnet is not lower than 1000 ppm. Because the extremely high hydroxyl contents are only associated with a few data-points, a conservative estimation of the maximum hydroxyl content is about 1200 ppm for garnet. Taking into account the FTIR analytical uncertainties, 1000 ppm H_2O was assumed as the initial water content for garnet. Omphacites from Dabie-Sulu eclogites have hydroxyl contents of 115–1300 ppm H_2O (Zhang et al., 2001, 2004; Sheng et al., 2007). Omphacite from the CCSD-MH eclogites has structural hydroxyl contents in the range of 228–412 ppm (this study). Thus, the maximum water content of 1300 ppm was used as the initial water content for omphacite.

(2) *Remaining water content*. The garnet from the two core segments of CCSD-MH has structural hydroxyl contents of 80 to 413 ppm H_2O (Table 2), but most of them are about 240 ppm. Thus, H_2O content of 240 ppm was assumed to be the remaining water content for garnet. The omphacite has structural hydroxyl contents of 228–412 ppm H_2O (Table 3); four samples I-6A, I-10A, I-11A and I-13A have relatively higher water contents of 319–412 ppm, but others have relatively homogeneous water contents of about 260 ppm. Hence, water content of 260 ppm was taken as the remaining water content for omphacite.

(3) *Mineral density*. Garnet and omphacite have many end-members of chemical composition. In order to obtain the densities of garnet and omphacite, we need to know their chemical compositions in the CCSD-MH samples. Mineral chemistry analysis was performed by Zhang et al. (2006), and the results indicate that the garnet in eclogite at the depth of 930 m is composed of 2.7% pyrope, 40.5% grossular, 46.5% almandine and 10.3% spessartine. Thus, we assume that the garnets from the two core segments have a composition of 5% pyrope, 40% grossular, 45% almandine and 10% spessartine. The densities of the four end-members of garnet are 3.56 g cm^{-3} for pyrope, 3.60 g cm^{-3} for grossular, 4.31 g cm^{-3} for almandine and 4.20 g cm^{-3} for spessartine. As a result, a density of 3.98 g cm^{-3} for garnet was obtained by calculating the weighted mean. Omphacite in the eclogite at the depth of 731 m consists of 48% jadeite, 46% diopside and 7% hedenbergite (Zhang et al., 2006). Hence, the omphacites from the two core segments were assumed to have a composition of 45% jadeite, 45% diopside and 10% hedenbergite. The densities of jadeite, diopside and hedenbergite are 3.34, 3.27 and 3.66 g cm^{-3}, respectively. Thus, a density of 3.35 g cm^{-3} for omphacite was obtained by calculating the weighted mean.

On the basis of the above assumptions, we have calculated the amount of water that can be released from eclogite that is the size of a hand specimen ($3 \times 6 \times 9$ cm^3) and 1 m^3 with different proportions of garnet and omphacite (Table 4). It appears that the decompression exsolution of structural hydroxyl from the eclogites that are hand-specimen size and 1 m^3 volume can release 0.078–0.101 wt% H_2O (in amounts of 0.497–0.557 g and 3.07–3.44 kg, respectively, for the two volumes of eclogite). If these amounts of released water are consumed to produce amphibole, we can also calculate how much hornblende can form in the eclogites by dividing by the water content of amphibole. According to the chemical formulas of different amphiboles, their H_2O contents (wt) vary from ~1.8% to ~2.2% for tremolite-actinolite, from ~1.8% to ~2.2% for hornblende and from ~1.9% to ~2.3% for glaucophane. Thus, amphibole was assumed to have a water content of 2.2% by weight (e.g., Schmidt and Poli, 2003).

As listed in Table 4, the hand specimen of eclogite composed of 50% garnet and 50% omphacite can release 0.527 g water, which can form 24.0 g amphibole during exhumation. The 1 m^3 of eclogite having the same composition

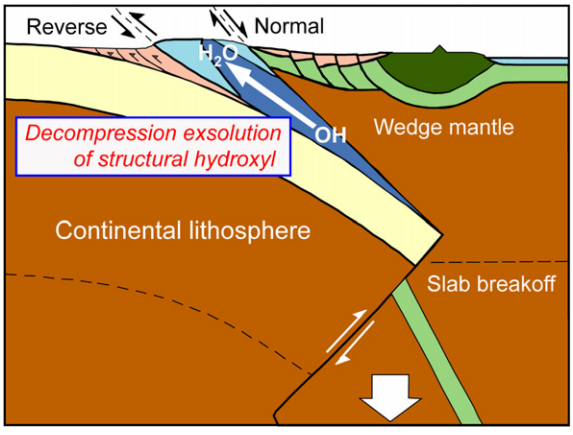

Fig. 12. A geodynamic model of water loss by decompression exsolution of structural hydroxyl from minerals during exhumation of deeply subducted continental crust.

Table 4
Estimate of water amounts by hydroxyl exsolution from eclogite minerals during exhumation

Garnet (vol %)	Omphacite (vol %)	Rock weight (kg)	Initial H_2O weight (kg)			Remaining H_2O weight (kg)			H_2O loss (kg)	Hornblende (kg)	Whole-rock H_2O (wt%)		
			Garnet	Omphacite	Whole-rock	Garnet	Omphacite	Whole-rock			Before	After	Loss
3 × 6 × 9 cm³													
10	90	0.553	6.45E−05	6.35E−04	6.99E−04	1.55E−05	1.27E−04	1.42E−04	5.57E−04	0.0253	0.127	0.026	0.101
20	80	0.563	1.29E−04	5.64E−04	6.93E−04	3.09E−05	1.13E−04	1.44E−04	5.50E−04	0.0250	0.123	0.026	0.098
30	70	0.573	1.93E−04	4.94E−04	6.87E−04	4.64E−05	9.88E−05	1.45E−04	5.42E−04	0.0246	0.120	0.025	0.095
40	60	0.584	2.58E−04	4.23E−04	6.81E−04	6.19E−05	8.47E−05	1.47E−04	5.35E−04	0.0243	0.117	0.025	0.092
50	50	0.594	3.22E−04	3.53E−04	6.75E−04	7.74E−05	7.06E−05	1.48E−04	5.27E−04	0.0240	0.114	0.025	0.089
60	40	0.604	3.87E−04	2.82E−04	6.69E−04	9.28E−05	5.64E−05	1.49E−04	5.20E−04	0.0236	0.111	0.025	0.086
70	30	0.614	4.51E−04	2.12E−04	6.63E−04	1.08E−04	4.23E−05	1.51E−04	5.12E−04	0.0233	0.108	0.025	0.083
80	20	0.624	5.16E−04	1.41E−04	6.57E−04	1.24E−04	2.82E−05	1.52E−04	5.05E−04	0.0229	0.105	0.024	0.081
90	10	0.635	5.80E−04	7.06E−05	6.51E−04	1.39E−04	1.41E−05	1.53E−04	4.97E−04	0.0226	0.103	0.024	0.078
1 m³													
10	90	3413	0.40	3.92	4.32	0.10	0.78	0.88	3.44	156.28	0.127	0.026	0.101
20	80	3476	0.80	3.48	4.28	0.19	0.70	0.89	3.39	154.19	0.123	0.026	0.098
30	70	3539	1.19	3.05	4.24	0.29	0.61	0.90	3.35	152.10	0.120	0.025	0.095
40	60	3602	1.59	2.61	4.21	0.38	0.52	0.90	3.30	150.01	0.117	0.025	0.092
50	50	3665	1.99	2.18	4.17	0.48	0.44	0.91	3.25	147.93	0.114	0.025	0.089
60	40	3728	2.39	1.74	4.13	0.57	0.35	0.92	3.21	145.84	0.111	0.025	0.086
70	30	3791	2.79	1.31	4.09	0.67	0.26	0.93	3.16	143.75	0.108	0.025	0.083
80	20	3854	3.18	0.87	4.06	0.76	0.17	0.94	3.12	141.67	0.105	0.024	0.081
90	10	3917	3.58	0.44	4.02	0.86	0.09	0.95	3.07	139.58	0.103	0.024	0.078

The calculations assume the initial hydroxyl contents of 1000 ppm H_2O wt for garnet and 1300 ppm H_2O wt for omphacite, and the remaining hydroxyl contents of 240 ppm H_2O wt for garnet and 260 ppm H_2O wt for omphacite. Mineral end-member compositions were used to calculate average densities, yielding 3.98 g cm^{-3} for garnet and 3.35 g cm^{-3} for omphacite. Amphibole is assumed to have a water content of 2.2% by weight. The lost H_2O amounts for whole-rock are calculated from the two cases before and after dehydration.

Table 5
Estimate of water amounts by decompression exsolution of both molecular water and structural hydroxyl from eclogite minerals during exhumation

Garnet (vol %)	Omphacite (vol %)	Rock weight (kg)	Initial H_2O weight (kg)			Remaining H_2O weight (kg)			H_2O loss (kg)	Hornblende (kg)	Whole-rock H_2O (wt%)		
			Garnet	Omphacite	Whole-rock	Garnet	Omphacite	Whole-rock			Before	After	Loss
3 × 6 × 9 cm^3													
10	90	0.553	7.74E−05	1.12E−03	1.20E−03	1.55E−05	1.27E−04	1.42E−04	1.06E−03	0.0481	0.217	0.026	0.191
20	80	0.563	1.55E−04	9.99E−04	1.15E−03	3.09E−05	1.13E−04	1.44E−04	1.01E−03	0.0459	0.205	0.026	0.179
30	70	0.573	2.32E−04	8.74E−04	1.11E−03	4.64E−05	9.88E−05	1.45E−04	9.61E−04	0.0437	0.193	0.025	0.168
40	60	0.584	3.09E−04	7.49E−04	1.06E−03	6.19E−05	8.47E−05	1.47E−04	9.12E−04	0.0414	0.181	0.025	0.156
50	50	0.594	3.87E−04	6.24E−04	1.01E−03	7.74E−05	7.06E−05	1.48E−04	8.63E−04	0.0392	0.170	0.025	0.145
60	40	0.604	4.64E−04	4.99E−04	9.64E−04	9.28E−05	5.64E−05	1.49E−04	8.14E−04	0.0370	0.160	0.025	0.135
70	30	0.614	5.42E−04	3.74E−04	9.16E−04	1.08E−04	4.23E−05	1.51E−04	7.65E−04	0.0348	0.149	0.025	0.125
80	20	0.624	6.19E−04	2.50E−04	8.69E−04	1.24E−04	2.82E−05	1.52E−04	7.17E−04	0.0326	0.139	0.024	0.115
90	10	0.635	6.96E−04	1.25E−04	8.21E−04	1.39E−04	1.41E−05	1.53E−04	6.68E−04	0.0304	0.129	0.024	0.105
1 m^3													
10	90	3413	0.48	6.93	7.41	0.10	0.78	0.88	6.53	296.94	0.217	0.026	0.191
20	80	3476	0.96	6.16	7.12	0.19	0.70	0.89	6.23	283.24	0.205	0.026	0.179
30	70	3539	1.43	5.39	6.83	0.29	0.61	0.90	5.93	269.55	0.193	0.025	0.168
40	60	3602	1.91	4.62	6.53	0.38	0.52	0.90	5.63	255.85	0.181	0.025	0.156
50	50	3665	239	3.85	6.24	0.48	0.44	0.91	5.33	242.15	0.170	0.025	0.145
60	40	3728	2.87	3.08	5.95	0.57	0.35	0.92	5.03	228.46	0.160	0.025	0.135
70	30	3791	3.34	2.31	5.65	0.67	0.26	0.93	4.72	214.76	0.149	0.025	0.125
80	20	3854	3.82	1.54	5.36	0.76	0.17	0.94	4.42	201.07	0.139	0.024	0.115
90	10	3917	4.30	0.77	5.07	0.86	0.09	0.95	4.12	187.37	0.129	0.024	0.105

The calculations assume the initial contents of 1200 ppm H_2O wt for garnet and 2300 ppm H_2O wt for omphacite, and the remaining hydroxyl contents of 240 ppm H_2O wt for garnet and 260 ppm H_2O wt for omphacite. Mineral end-member compositions were used to calculate average densities, yielding 3.98 g cm^{-3} for garnet and 3.35 g cm^{-3} for omphacite. Amphibole is assumed to have a water content of 2.2% by weight. The lost H_2O amounts for whole-rock are calculated from the two cases before and after dehydration.

can deliver 3.25 kg water to form 147.93 kg amphibole. This delivers a sufficient amount of water for amphibolitization, and some could be focused to form quartz veins within UHP eclogites. Beside garnet and omphacite, in fact, eclogite usually contains minor amounts of hydrous minerals (e.g., phengite ± epidote) and other nominally anhydrous minerals (e.g., rutile ± kyanite ± quartz). They can also significantly dehydrate during exhumation, sometimes releasing even more water than those from garnet and omphacite. In this regard, the present calculation only provides the minimum estimate of water amounts that would be lost from the eclogites during exhumation. In either case, the present study demonstrates that significant amounts of aqueous fluid can be released from nominally anhydrous minerals by the decompression exsolution of structural hydroxyl during the exhumation of deeply subducted continental crust (Fig. 12).

It is possible that molecular H_2O was also released from the minerals during exhumation because the molecular H_2O is neutral with a smaller size and thus more mobile than the structural OH bounded to mineral structures. As a result, the nominally anhydrous minerals can release more water than the present estimation. By changing the initial water contents of garnet and omphacite, the water loss from eclogite by exsolution of both molecular water and structural hydroxyl was estimated. The total water contents in garnet from the CCSD-MH eclogites range from 522 to 1251 ppm, thus 1200 ppm was taken as the initial water content for garnet. Except for several data of high total water contents that were certainly caused by retrograde metamorphism, omphacite has total water contents of 1170–2376 ppm. Thus, 2300 ppm H_2O was taken as the initial water content for omphacite. The other assumptions were taken in a similar manner as those used in the above estimation of hydroxyl exsolution. The results show that the hand specimen of eclogite composed of 50% garnet and 50% omphacite can release 0.863 g water, which can form 39.2 g amphibole during exhumation. The 1 m^3 of eclogite having the same composition can deliver 5.33 kg water to form 242.15 kg amphibole (Table 5). On the other hand, if fluid inclusions were formed from some of the fluid released from the nominally anhydrous minerals by the decompression exsolution of structural hydroxyl, the amounts of amphibole formed by this way would be smaller than the estimates.

Gneiss commonly contains conspicuous amounts of hydrous minerals (e.g., micas ± epidote). The other nominally anhydrous minerals (e.g., feldspar + quartz ± magnetite) in the gneiss can also contain considerable amounts of structural hydroxyl and molecular H_2O (Nakashima et al., 1995; Rossman, 1996; Grant et al., 2003; Bell et al., 2004; Johnson and Rossman, 2004). In addition, TC/EA-MS analysis for UHP metamorphic rocks at Taohang in the Sulu orogen shows that gneiss minerals contain large amounts of the total water in feldspar and magnetite (Gong et al., 2007b). Therefore, the gneiss is capable of storing more water than the eclogite under the same UHP conditions. Thus, the UHP gneiss can release more water than the UHP eclogite during the initial exhumation of deeply subducted slabs. By decompression dehydration at the contact between eclogite and gneiss, the released water could flow from the gneiss to the eclogite and result in remarkable hydration of the eclogite adjacent to the gneiss.

6. CONCLUSIONS

The TC/EA-MS technique has been successfully applied to analyses of both H isotope composition and total H_2O concentration of nominally anhydrous minerals in UHP eclogite and gneiss from two continuous CCSD-MH core segments. The results show variable δD values of −116‰ to −64‰ for garnet and −104‰ to −82‰ for omphacite. These δD values are consistent with previous measurements of hydrous minerals by conventional extraction methods. This serves to verify incorporation of meteoric water into protoliths of UHP metaigneous rocks by high-T hydrothermal alteration and subsequent magmatism. Both equilibrium and re-equilibrium H isotope fractionations occur between garnet and omphacite in the first core segment. The eclogites away from the boundary between eclogite and gneiss mostly have H isotope fractionations of about 14‰ between garnet and omphacite, corresponding to equilibrium values acquired during the eclogite-facies metamorphism. On the other hand, the eclogites adjacent to gneiss show H isotope fractionations of about 4‰ between garnet and omphacite, pointing to retrograde re-equilibrium under amphibolite-facies conditions during exhumation. For the second core segment, the garnet amphibolites show H isotope compositions similar to those for the gneisses. H isotope fractionations between garnet and omphacite for the eclogites indicate that H isotope exchange between garnet and omphacite occurs in a relatively closed system.

Significant amounts of water are found in garnets from the eclogites, garnet amphibolites and gneisses and in omphacites from the eclogites. TC/EA-MS analyses yielded total water contents of 522–1584 ppm in garnet and 1170–20745 ppm in omphacite, whereas FTIR analyses gave hydroxyl concentrations of 80–413 ppm for garnet and 228–412 ppm for omphacite. On one hand, the difference in mineral water content between the measurements by the two methods demonstrates the presence of molecular water in the UHP eclogite minerals, and thus suggests enhanced capacity of water storage in the mantle. On the other hand, the hydroxyl contents only provide the lower limits of actual dissolved hydroxyl in the nominally anhydrous minerals at mantle depths because large fractions of water escaped upon decompression exsolution. Both TC/EA-MS and FTIR analyses show that garnet from the gneisses contains more water than that from the eclogites. In accordance with the petrographic observations that show an increased degree of retrograde metamorphism with decreasing distance from the eclogite–gneiss boundary, it appears that retrograde metamorphism results in mineral reactions and δD variation at the transition between different lithologies. For the eclogites adjacent to the gneisses, the fluid for retrogression was mainly derived from the gneisses. In contrast, the eclogites away from the boundary between eclogite and gneiss may have retrograde fluid that is locally derived from the eclogites themselves by the decompression exsolution of structural hydroxyl during

exhumation. A quantitative estimate suggests that a 1 m^3 volume of bimineral eclogite composed of garnet and omphacite can release 3.07–3.44 kg of water by the decompression exsolution of structural hydroxyl, which can in turn form 139.58–156.28 kg of amphibole during exhumation. This can provide a sufficient amount of water for amphibolitization of UHP eclogites.

ACKNOWLEDGMENTS

This study has been supported by funds from the National Ministry of Science and Technology (2003CB716501) and the Natural Science Foundation of China (40573011). Thanks are due to Qunke Xia, Yingming Sheng and Xiaozhi Yang for their assistance with FTIR analysis. Comments by D.R. Cole, J.G. Liou and two anonymous reviewers helped improve the presentation.

REFERENCES

Aines R. D., and Rossman G. R. (1984a) The hydrous component in garnets: pyraspites. *Am. Mineral.* **69**, 1116–1126.

Aines R. D., and Rossman G. R. (1984b) Water content of mantle garnets. *Geology* **12**, 720–723.

Ames L., Zhou G.-Z., and Xiong B.-C. (1996) Geochronology and isotopic character of ultrahigh-pressure metamorphism with implications for the collision of the Sino-Korean and Yangtze cratons, central China. *Tectonics* **15**, 472–489.

Amthauer G., and Rossman G. R. (1998) The hydrous component in andradite garnet. *Am. Mineral.* **83**, 835–840.

Aoki I., and Takahashi E. (2004) Density of MORB eclogite in the upper mantle. *Phys. Earth Planet. Inter.* **143**, 129–143.

Baker J., Matthews A., Mattey D., Rowley D., and Xue F. (1997) Fluid-rock interactions during ultra-high pressure metamorphism, Dabie Shan, China. *Geochim. Cosmochim. Acta* **61**, 1658–1696.

Begley I. S., and Scrimgeour C. M. (1997) High-precision δ^2H and $\delta^{18}O$ measurement for water and volatile organic compounds by continuous-flow pyrolysis isotope ratio mass spectrometry. *Anal. Chem.* **69**, 1530–1535.

Bell D. R., and Rossman G. R. (1992a) Water in the earth's mantle: the role of nominally anhydrous minerals. *Science* **255**, 1391–1397.

Bell D. R., and Rossman G. R. (1992b) The distribution of hydroxyl in garnets from the sub-continental mantle of southern Africa. *Contrib. Mineral. Petrol.* **111**, 161–178.

Bell D. R., Ihinger P. D., and Rossman G. R. (1995) Quantitative analysis of hydroxyl in garnet and pyroxene. *Am. Mineral.* **80**, 465–474.

Bell D. R., and Ihinger P. D. (2000) The isotope composition of hydrogen in nominally anhydrous mantle minerals. *Geochim. Cosmochim. Acta* **64**, 2109–2118.

Bell D. R., Rossman G. R., and Moore R. O. (2004) Abundance and partitioning of OH in a high-pressure magmatic system: megacrysts from the Monastery kimberlite, South Africa. *J. Petrol.* **45**, 1539–1564.

Beran A., Langer K., and Andrut M. (1993) Single crystal infrared spectra in the range of OH fundamentals of paragenetic garnet, omphacite and kyanite in an eclogitic mantle xenoliths. *Mineral. Petrol.* **48**, 257–268.

Blanchard M., and Ingrin J. (2004a) Kinetics of deuteration in pyrope. *Eur. J. Mineral.* **16**, 567–576.

Blanchard M., and Ingrin J. (2004b) Hydrogen diffusion in Dora Maira pyrope. *Phys. Chem. Miner.* **31**, 593–605.

Bolfan-Casanova N. (2005) Water in the Earth's mantle. *Mineral. Mag.* **69**, 229–257.

Bromiley G. D., and Keppler H. (2004) An experimental investigation of hydroxyl solubility in jadeite and Na-rich clinopyroxenes. *Contrib. Mineral. Petrol.* **147**, 189–200.

Bromiley G. D., Keppler H., McCammon C., Bromiley F. A., and Jacobsen S. D. (2004a) Hydrogen solubility and speciation in natural, gem-quality chromian diopside. *Am. Mineral.* **89**, 941–949.

Bromiley G., Hilaret N., and McCammon C. (2004b) Solubility of hydrogen and ferric iron in rutile and TiO_2 (II): implications for phase assemblages during ultrahigh-pressure metamorphism and for the stability of silica polymorphs in the lower mantle. *Geophys. Res. Lett.* **31**, L04610. doi:10.1029/2004GL01943.

Burgoyne T. W., and Hayes J. M. (1998) Quantitative production of H_2 by pyrolysis of gas chromatographic effluents. *Anal. Chem.* **70**, 5136–5141.

Cong B.-L. (1996) *Ultrahigh-Pressure Metamorphic Rocks in the Dabieshan-Sulu Region of China*. Science Press, Beijing, 224pp.

Doremus R. H. (2004) Transport of oxygen in silicate glasses. *J. Non-Crys. Solids* **349**, 242–247.

Eiler J. M., and Kitchen N. (2001) Hydrogen-isotope analysis of nanomole (picoliter) quantities of H_2O. *Geochim. Cosmochim. Acta* **65**, 4467–4479.

Enami M., Cong B. L., Yoshida T., and Kawabe I. (1995) A mechanism for Na incorporation in garnet: an example from garnet in orthogneiss from the Su-Lu terrane, eastern China. *Am. Mineral.* **80**, 475–482.

Farver J. R., and Gilletti B. J. (1985) Oxygen diffusion in amphiboles. *Geochim. Cosmochim. Acta* **49**, 1403–1411.

Fortier S. M., and Gilletti B. J. (1989) An empirical model for predicting diffusion coefficients in silicate minerals. *Science* **245**, 1481–1484.

Fortier S. M., and Gilletti B. J. (1991) Volume self-diffusion of oxygen in biotite, muscovite, and phlogopite micas. *Geochim. Cosmochim. Acta* **55**, 1319–1330.

Franz L., Romer R. L., Klemd R., Schmid R., Oberhansli R., Wanger T., and Dong S. W. (2001) Eclogite-facies quartz veins within metabasites of the Dabie Shan (eastern China): pressure–temperature–time–deformation path, composition of the fluid phase and fluid flow during exhumation of high-pressure rocks. *Contrib. Mineral. Petrol.* **141**, 322–346.

Freer R. (1981) Diffusion in silicate minerals and glasses: a data digest and guide to the literature. *Contrib. Mineral. Petrol.* **76**, 440–454.

Fu B., Zheng Y.-F., Wang Z.-R., Xiao Y.-L., Gong B., and Li S.-G. (1999) Oxygen and hydrogen isotope geochemistry of gneisses associated with ultrahigh pressure pressure eclogites at Shuanghe in the Dabie Mountains. *Contrib. Mineral. Petrol.* **134**, 52–66.

Fu B., Touret J. L. R., and Zheng Y.-F. (2001) Fluid inclusions in coesite-bearing eclogites and jadeite quartzites at Schuanghe, Dabie Shan, China. *J. Metamorph. Geol.* **19**, 531–548.

Fu B., Zheng Y.-F., and Touret J. L. R. (2002) Petrological, isotopic and fluid inclusion studies of eclogites from Sujiahe, NW Dabie Shan (China). *Chem. Geol.* **187**, 107–128.

Fu B., Touret J. L. R., and Zheng Y.-F. (2003a) Remants of premetamorphic fluid and oxygen isotopic signatures in eclogites and garnet clinopyroxenite from the Dabie-Sulu terranes, eastern China. *J. Metamorph. Geol.* **21**, 561–578.

Fu B., Touret J. L. R., Zheng Y.-F., and Jahn B.-m. (2003b) Fluid inclusions in granulites, granulitized eclogites, and garnet clinopyroxenites from the Dabie-Sulu terranes, eastern China. *Lithos* **70**, 293–319.

Godin J. P., Richelle M., Metairon S., and Fay L. B. (2004) [$^2H/H$] isotope ratio analyses of [$^2H_5$] cholesterol using high-temperature conversion elemental analyser isotope-ratio mass spectrometry: determination of cholesterol absorption in

normocholesterolemic volunteers. *Rapid Commun. Mass Spectrom.* **18**, 325–330.

Gong B., Zheng Y.-F., and Chen R.-X. (2007a). An online method combining a thermal conversion elemental analyzer with isotope ratio mass spectrometry for the determination of hydrogen isotope composition and water concentration in geological samples. *Rapid Commun. Mass Spectrom.* **21**, doi:10.1002/rcm.2973.

Gong, B., Zheng, Y.-F., Wu, Y.-B., Zhao, Z.-F., Gao, T.-S., Tang, J., Chen, R.-X., Fu, B., and Liu, X.-M. (2007b). Geochronology and stable isotope geochemistry of UHP metamorphic rocks at Taohang in the Sulu orogen, east-central China. *Int. Geol. Rev.* **49,** in press.

Grant K., Gleeson S. A., and Roberts S. (2003) The high-temperature behavior of defect hydrogen species in quartz: implications for hydrogen isotope studies. *Am. Mineral.* **88**, 262–270.

Hacker B. R., Ratschbacher L., Webb L., Ireland T., Walker D., and Dong S. (1998) U/Pb zircon ages constrain the architecture of the ultrahigh-pressure Qinling-Dabie Orogen, China. *Earth Planet. Sci. Lett.* **161**, 215–230.

Hacker B. R., Ratschbacher L., Webb L., McWilliams M. O., Ireland T., Calvert A., Dong S., Wenk H.-R., and Chateigner D. (2000) Exhumation of ultrahigh-pressure continental crust in east central China: Late Triassic–Early Jurassic tectonic unroofing. *J. Geophys. Res.* **B105**, 13339–13364.

Hauri E. H., Gaetani G. A., and Green T. H. (2006) Partitioning of water during melting of the Earth's upper mantle at H_2O-undersaturated conditions. *Earth Planet. Sci. Lett.* **248**, 715–734.

Hilkert A. W., Douthitt C. B., Schlueter H. J., and Brand W. A. (1999) Isotope ratio monitoring gas chromatography/mass spectrometry of D/H by high temperature conversion isotope ratio mass spectrometry. *Rapid Commun. Mass spectrom.* **13**, 1226–1230.

Ingrin J., Hercule S., and Charton T. (1995) Diffusion of hydrogen in diopside: results of dehydration experiments. *J. Geophys. Res.* **100**, 15489–15499.

Ingrin J., and Skogby H. (2000) Hydrogen in nominally anhydrous upper-mantle minerals: concentration levels and implications. *Eur. J. Mineral.* **12**, 543–570.

Johnson E. A., and Rossman G. R. (2004) A survey of hydrous species and concentrations in igneous feldspars. *Am. Mineral.* **89**, 586–600.

Katayama I., and Nakashima S. (2003) Hydroxyl in clinopyroxene from the deep subducted crust: evidence for H_2O transport into the mantle. *Am. Mineral.* **88**, 229–234.

Katayama I., Nakashima S., and Yurimoto H. (2006) Water content in natural eclogite and implication for water transport into the deep upper mantle. *Lithos* **86**, 245–259.

Koch-Muller M., Dera P., Fei Y. W., Reno B., Sobolev N., Hauri E., and Wysoczanski R. (2003) OH^- in synthetic and natural coesite. *Am. Mineral.* **88**, 1436–1445.

Langer K., Robarick E., Sobolev N. V., Shatsky V. S., and Wang W. (1993) Single-crystal spectra of garnets from diamondiferous high-pressure metamorphic rocks from Kazakhstan: indications for OH^-, H_2O, and FeTi charge transfer. *Eur. J. Mineral.* **5**, 1091–1100.

Li S.-G., Jagoutz E., Lo C.-H., Chen Y.-Z., Li Q.-L., and Xiao Y.-L. (1999) Sm/Nd, Rb/Sr, and $^{40}Ar/^{39}Ar$ isotopic systematics of the ultrahigh-pressure metamorphic rocks in the Dabie-Sulu belt, Central China: a retrospective view. *Int. Geol. Rev.* **41**, 1114–1124.

Li S.-G., Jagoutz E., Chen Y.-Z., and Li Q.-L. (2000) Sm-Nd and Rb-Sr isotopic chronology and cooling history of ultrahigh pressure metamorphic rocks and their country rocks at Shuanghe in the Dabie Mountains, Central China. *Geochim. Cosmochim. Acta* **64**, 1077–1093.

Li X.-P., Zheng Y.-F., Wu Y.-B., Chen F.-K., Gong B., and Li Y.-L. (2004) Low-T eclogite in the Dabie terrane of China: petrological and isotopic constraints on fluid activity and radiometric dating. *Contrib. Mineral. Petrol.* **148**, 443–470.

Liou J. G., Zhang R. Y., and Ernst W. G. (1995) Occurrences of hydrous and carbonate phases in ultrahigh-pressure rocks from east-central China: implications for the role of volatiles deep in cold subduction zone. *Islands Arc* **4**, 362–375.

Liou J. G., and Zhang R. Y. (1996) Occurrence of intergranular coesite in ultrahigh-pressure rocks from the Sulu region, eastern China: implication for lack of fluid during exhumation. *Am. Mineral.* **81**, 1217–1221.

Liou J. G., Zhang R. Y., Eide E. A., Wang X. M., Ernst W. G., and Maruyama, S. (1996) Metamorphism and tectonics of high-pressure and ultra-high-belts in the Dabie-Sulu region, China. In *The Tectonics of Asia* (eds. M.T. Harrison and A. Yin). Cambridge University Press, Cambridge, pp. 300–344.

Liu F.-L., Xu Z.-Q., Katayama I., Yang J. S., Maruyama S., and Liou J. G. (2001) Mineral inclusions in zircons of para- and orthogneiss from pre-pilot drillhole CCSD-PP1, Chinese Continental Scientific Drilling Project. *Lithos* **59**, 199–215.

Liu F.-L., and Xu Z.-Q. (2004) Fluid inclusions hidden in coesite-bearing zircons in ultrahigh-pressure metamorphic rocks from southwestern Sulu terrane in eastern China. *Chinese Sci. Bull.* **49**, 396–404.

Liu F.-L., Xu Z.-Q., and Xue H. M. (2004a) Tracing the protolith, UHP metamorphism, and exhumation ages of orthogneiss from the SW Sulu terrane (eastern China): SHRIMP U-Pb dating of mineral inclusion-bearing zircons. *Lithos* **78**, 411–429.

Liu F.-L., Xu Z.-Q., Liou J. G., and Song B. (2004b) SHRIMP U-Pb ages of ultrahigh-pressure and retrograde metamorphism of gneisses, south-western Sulu terrane, eastern China. *J. Metamorph. Geol.* **22**, 315–326.

Lu R., and Keppler H. (1997) Water solubility in pyrope to 100 kbar. *Contrib. Mineral. Petrol.* **129**, 35–42.

Matsyuk S. S., Langer K., and Hosch A. (1998) Hydroxyl defects in garnets from mantle xenoliths in kimberlites of the Siberian platform. *Contrib. Mineral. Petrol.* **132**, 163–179.

Mierdel K., and Keppler H. (2004) The temperature dependence of water solubility in enstatite. *Contrib. Mineral. Petrol.* **148**, 305–311.

Miller J. A., Buick I. S., Cartwright I., and Barnicoat A. (2002) Fluid processes during the exhumation of high-P metamorphic belts. *Mineral. Mag.* **12**, 827–840.

Mosenfelder J. L. (2000) Pressure dependence of hydroxyl solubility on coesite. *Phys. Chem. Miner.* **27**, 610–617.

Nakashima S., Matayoshi H., Yuko T., Michibayashi K., Masuda T., Kuroki N., Yamagishi H., Ito Y., and Nakamora A. (1995) Infrared microspectroscopy analysis of water distribution in deformed and metamorphosed rocks. *Tectonophysics* **245**, 263–276.

Newman S., Epstein S., and Stolper E. (1988) Water, carbon dioxide, and hydrogen isotopes in glasses from the ca. 1340 A.D. eruption of the Mono craters, California: constraints on degassing phenomena and initial volatile content. *J. Volcanol. Geotherm. Res.* **35**, 75–96.

Okamoto K., and Maruyama S. (2004) The eclogite–garnetite transition in the MORB + H_2O system. *Phys. Earth Planet. Inter.* **146**, 283–296.

Okay A. I., Xu S.-T., and Sengor A. M. C. (1989) Coesite from the Dabie Shan eclogites, central China. *Eur. J. Mineral.* **1**, 595–598.

Paterson M. S. (1982) The determination of hydroxyl by infrared absorption in quartz, silicate glasses and similar materials. *Bull. Mineral.* **105**, 20–29.

Pertermann M., and Hirschmann M. M. (2003) Anhydrous partial melting experiments on MORB-like eclogite: phase relations, phase compositions and mineral-melt partitioning of major elements at 2–3 GPa. *J. Petrol.* **44**, 2173–2201.

Rauch M., and Keppler H. (2002) Water solubility in orthopyroxene. *Contrib. Mineral. Petrol.* **143**, 525–536.

Rossman G. R., and Aines R. D. (1991) The hydrous components in garnets: grossular–hydrogrossular. *Am. Mineral.* **76**, 1153–1164.

Rossman G. R., Beran A., and Langer K. (1989) The hydrous component of pyrope from the Dora Maira Massif, Western Alps. *Eur. J. Mineral.* **1**, 151–154.

Rossman G. R. (1996) Studies of OH in nominally anhydrous minerals. *Phys. Chem. Miner.* **23**, 299–304.

Rumble D., and Yui T.-F. (1998) The Qinglongshan oxygen and hydrogen isotope anomaly near Donghai in Jiangsu province, China. *Geochim. Cosmochim. Acta* **62**, 3307–3321.

Rumble D., Giorgis D., Oreland T., Zhang Z.-M., Xu H.-F., Yui T.-F., Yang J.-S., Xu Z.-Q., and Liou J. G. (2002) Low $\delta^{18}O$ zircons, U–Pb dating, and the age of the Qinglongshan oxygen and hydrogen isotope anomaly near Donghai in Jiangsu province, China. *Geochim. Cosmochim. Acta* **66**, 2299–2306.

Schmidt M., and Poli S. (1998) Experimentally based water budgets for dehydrating slabs and consequences for arc magma generation. *Earth Planet. Sci. Lett.* **163**, 361–379.

Schmidt M. W., and Poli S. (2003) Generation of mobile components during subduction of oceanic crust. *Treatise Geochem.* **3**, 567–591.

Sharp Z. D., Atudorei V., and Durakiewicz T. (2001) A rapid method for determination of hydrogen and oxygen isotope ratios from water and hydrous minerals. *Chem. Geol.* **178**, 197–210.

Sheng Y. M., Xia Q. K., Dallai L., Yang X. Z., and Hao Y. T. (2007) H_2O contents and D/H ratios of nominally anhydrous minerals from ultrahigh-pressure eclogites of the Dabie orogen, eastern China. *Geochim. Cosmochim. Acta* **71**, 2079–2103.

Skogby H., Bell D. R., and Rossman G. R. (1990) Hydroxide in pyroxene: variation in the natural environment. *Am. Mineral.* **75**, 764–774.

Smyth J. R., Bell D. R., and Rossman G. R. (1991) Incorporation of hydroxyl in upper mantle clinopyroxenes. *Nature* **351**, 732–734.

Snyder G. A., Taylor L. A., Clayton R. N., Mayeda P., Deines P., Rossman G. R., and Sobolev N. V. (1995) Archean mantle heterogeneity and the origin of diamondiferous eclogites, Siberia: evidence from stable isotopes and hydroxyl in garnet. *Am. Mineral.* **80**, 799–809.

Stalder R., and Skogby H. (2003) Hydrogen diffusion in natural and synthetic orthopyroxene. *Phys. Chem. Miner.* **30**, 12–19.

Su W., You Z.-D., and Cong B.-L. (2002) Cluster of water molecules in garnet from ultrahigh-pressure eclogite. *Geology* **30**, 611–614.

Su W., Ji Z. P., You Z.-D., Liu J. B., Yu J., and Cong B. L. (2004) Distribution of hydrous components in jadeite of the Dabie Mountains. *Earth Planet. Sci. Lett.* **222**, 85–100.

Touret J. L. R. (2001) Fluids in metamorphic rocks. *Lithos* **55**, 1–25.

Wan Y. S., Li R. W., Wilde S. A., Liu D. Y., Chen Z. Y., Yan L. L., Song T. R., and Yin X. Y. (2005) UHP metamorphism and exhumation of the Dabie Orogen, China: evidence from SHRIMP dating of zircon and monazite from a UHP granitic gneiss cobble from the Hefei Basin. *Geochim. Cosmochim. Acta* **69**, 4333–4348.

Wang L. P., Zhang Y. X., and Essene E. J. (1996) Diffusion of the hydrous in pyrope. *Am. Mineral.* **81**, 706–718.

Wang X.-M., Liou J. G., and Mao H.-K. (1989) Coesite-bearing from the Dabie mountains in central China. *Geology* **17**, 1085–1088.

Wang X.-M., Zhang R. Y., and Liou J. G. (1995) UHPM terrane in east central China. In *Ultrahigh Pressure Metamorphism*, (eds. R. Coleman and X. Wang). Cambridge University Press, Cambridge, pp. 356–390.

Withers A. C., Wood B. J., and Carroll M. R. (1998) The OH content of pyrope at high pressure. *Chem. Geol.* **147**, 161–171.

Wu Y.-B., Zheng Y.-F., Zhao Z.-F., Gong B., Liu X.-M., and Wu F.-Y. (2006) U–Pb, Hf and O isotope evidence for two episodes of fluid-assisted zircon growth in marble-hosted eclogites from the Dabie orogen. *Geochim. Cosmochim. Acta* **70**, 3743–3761.

Xia Q.-K., Sheng Y.-M., Yang X.-Z., and Yu H.-M. (2005) Heterogeneity of water in garnets from UHP eclogites, eastern Dabieshan, China. *Chem. Geol.* **224**, 237–246.

Xiao Y. L., Hoefs J., van den Kerkhof A. M., Fieberg J., and Zheng Y.-F. (2000) Fluid history of UHP metamorphism in Dabie Shan, China: a fluid inclusion and oxygen isotope study on the coesite-bearing eclogite from Bixiling. *Contrib. Mineral. Petrol.* **139**, 1–16.

Xiao Y. L., Hoefs J., van den Kerkhof A. M., and Li S. (2001) Geochemical constraints of the eclogite and granulite facies metamorphism as recognized in Raobazhai complex from North Dabie Shan, China. *J. Metamorph. Geol.* **19**, 3–19.

Xiao Y. L., Hoefs J., van den Kerkhof A. M., Simon K., Fiebig J., and Zheng Y.-F. (2002) Fluid evolution during HP and UHP metamorphism in Dabie Shan, China: Constraints from mineral chemistry, fluid inclusion and stable isotopes. *J. Petrol.* **43**, 1505–1527.

Xiao Y. L., Zhang Z.-M., Hoefs J., and van den Kerkhof A. M. (2006) Ultrahigh-pressure metamorphic rocks from the Chinese Continental Scientific Drilling Project-II. Oxygen isotope and fluid inclusion distributions through vertical sections. *Contrib. Mineral. Petrol.* **152**, 443–458.

Xu S.-T., Okay A. I., Ji S.-Y., Sengor A. M. C., Su W., Liu Y.-C., and Jiang L.-L. (1992) Diamond from the Dabie Shan metamorphic rocks and its implication for tectonic setting. *Science* **256**, 80–82.

Xu Z.-Q., Yang W.-C., Zhang Z.-M., and Yang T. N. (1998) Scientific significance and site-selection researches of the first Chinese continental scientific deep drillhole. *Continental Dyn.* **3**, 1–13.

Xu S. T., Liu Y. C., Chen G. B., Roberto C., Franco R., He M. C., and Liu H. F. (2003) New finding of microdiamonds in eclogites from Dabie-Sulu region in central-eastern China. *Chinese Sci. Bull.* **48**, 988–994.

Xu Z.-Q., Zhang Z.-M., Liu F.-L., Yang J.-S., Tang Z.-M., Chen S.-Z., Cai Y.-C., Li T.-F., and Chen F.-Y. (2004) The structure profile of 0–1200 m in the main hole, Chinese Continental Scientific Drilling and its preliminary deformation analysis. *Acta Petrol. Sin. (in Chinese with English abstract)* **20**, 53–72.

Xu S.-T., Liu Y.-C., Chen G.-B., Ji S.-Y., Ni P., and Xiao W.-S. (2005) Microdiamonds, their classification and tectonic implications for the host eclogites from the Dabie and Su–Lu regions in central eastern China. *Mineral. Mag.* **69**, 509–520.

Ye K., Yao Y. P., Katayama I., Cong B. L., Wang Q. C., and Maruyama S. (2000) Large areal extent of ultrahigh-pressure metamorphism in the Sulu ultrahigh-pressure terrane of east China: new implications from coesite and omphacite inclusions in zircon of granitic gneiss. *Lithos* **52**, 157–164.

Yui T.-F., Rumble D., and Lo C.-H. (1995) Unusually low $\delta^{18}O$ ultra-high-pressure metamorphic rocks from the Sulu Terrane, eastern China. *Geochim. Cosmochim. Acta* **59**, 2859–2864.

Yui T.-F., Rumble D., Chen C.-H., and Lo C.-H. (1997) Stable isotope characteristics of eclogites from the ultra-high-pressure metamorphic terrain, east-central China. *Chem. Geol.* **137**, 135–147.

Zhang Y. X., Stolper E. M., and Wasserburg G. J. (1991) Diffusion of a multi-species component and its role in oxygen and water transport in silicates. *Earth Planet. Sci. Lett.* **103**, 228–240.

Zhang R. Y., Hirajima T., Banno S., Cong B. L., and Liou J. G. (1995) Petrology of ultrahigh-pressure rocks from the southern Su–Lu region, eastern China. *J. Metamorph. Geol.* **13**, 659–675.

Zhang Z.-M., Xu Z.-Q., and Xu H.-F. (2000) Petrology of ultrahigh-pressure eclogites from the ZK703 drillhole in the Donghai, eastern China. *Lithos* **52**, 35–50.

Zhang J. F., Jin Z. M., Green H. W., and Jin S. Y. (2001) Hydroxyl in continental deep subduction zone: evidence from UHP eclogites of the Dabie mountains. *Chinese Sci. Bull.* **46**, 592–595.

Zhang R. Y., Liou J. G., and Shu J. F. (2002) Hydroxyl-rich topaz in high-pressure and ultrahigh-pressure kyanite quartzites, with retrograde woodhouseite, from the Sulu terrane, eastern China. *Am. Mineral.* **87**, 445–453.

Zhang R. Y., Liou J. G., Zheng Y.-F., and Fu B. (2003) Transition of UHP eclogites to gneissic rocks of low-grade amphibolite facies during exhumation: evidence from the Dabie terrane, central China. *Lithos* **70**, 269–291.

Zhang J. F., Green H. W., Bozhilov K., and Jin Z. M. (2004) Faulting induced by precipitation of water at grain boundaries in hot subducting oceanic crust. *Nature* **428**, 633–636.

Zhang Z.-M., Xiao Y.-L., Xu Z.-Q., Hoefs J., Yang J.-S., Liu F.-L., Liou J. G., and Simons K. (2006) UHP metamorphic rocks from the Chinese continental scientific drilling project: I. petrology and geochemistry of the main hole ($0 \sim 2{,}050$ m). *Contrib. Mineral. Petrol.* **152**, 421–441.

Zhao Z.-F., Zheng Y.-F., Gao T.-S., Wu Y.-B., Chen B., Chen F. K., and Wu F.-Y. (2006) Isotopic constraints on age and duration of fluid-assisted high-pressure eclogite-facies recrystallization during exhumation of deeply subducted continental crust in the Sulu orogen. *J. Metamorph. Geol.* **24**, 687–702.

Zhao Z.-F., Chen B., Zheng Y.-F., Chen R.-X., and Wu Y.-B. (2007) Mineral oxygen isotope and hydroxyl content changes in ultrahigh-pressure eclogite–gneiss contacts from Chinese Continental Scientific Drilling Project cores. *J. Metamorph. Geol.* **25**, 165–186.

Zhao Z.-F., and Zheng Y.-F. (2007) Diffusion compensation for argon, hydrogen, lead and strontium in minerals: empirical relationship to crystal chemistry. *Am. Mineral.* **92**, 289–308.

Zheng Y.-F. (1992) Discussion on the use of $\delta - \Delta$ diagram in interpreting stable isotope data. *Eur. J. Mineral.* **4**, 635–643.

Zheng Y.-F., Fu B., Gong B., and Li S. (1996) Extreme ^{18}O depletion in eclogite from the Su-Lu terrane in East China. *Eur. J. Mineral.* **8**, 317–323.

Zheng Y.-F., and Fu B. (1998) Estimation of oxygen diffusivity from anion porosity in minerals. *Geochem. J.* **32**, 71–89.

Zheng Y.-F., Fu B., Li Y.-L., Xiao Y.-L., and Li S.-G. (1998) Oxygen and hydrogen isotope geochemistry of ultrahigh-pressure eclogites from the Dabie mountains and Sulu terrane. *Earth Planet. Sci. Lett.* **155**, 113–129.

Zheng Y.-F., Fu B., Xiao Y.-L., Li Y.-L., and Gong B. (1999) Hydrogen and oxygen isotope evidence for fluid–rock interactions in the stages of pre- and post-UHP metamorphism in the Dabie mountains. *Lithos* **46**, 677–693.

Zheng Y.-F., Fu B., Gong B., and Li L. (2003) Stable isotope geochemistry of ultrahigh pressure metamorphic rocks from the Dabie-Sulu orogen in China: implications for geodynamics and fluid regime. *Earth Sci. Rev.* **62**, 105–161.

Zheng Y.-F., Wu Y.-B., Chen F.-K., Gong B., Li L., and Zhao Z.-F. (2004) Zircon U–Pb and oxygen isotope evidence for a large-scale ^{18}O depletion event in igneous rocks during the Neoproterozoic. *Geochem. Cosmochim. Acta* **68**, 4145–4165.

Zheng Y.-F., Zhou J.-B., Wu Y.-B., and Xie Z. (2005a) Low-grade metamorphic rocks in the Dabie-Sulu orogenic belt: a passive-margin accretionary wedge deformed during continent subduction. *Int. Geol. Rev.* **47**, 851–871.

Zheng Y.-F., Wu Y.-B., Zhao Z.-F., Zhang S.-B., Xu P., and Wu F.-Y. (2005b) Metamorphic effect on zircon Lu-Hf and U-Pb isotope systems in ultrahigh-pressure eclogite-facies metagranite and metabasite. *Earth Planet. Sci. Lett.* **240**, 378–400.

Associate Editor: David R. Cole